e-Prime - Advances in Electrical Engineering, Electronics and Energy 13 (2025) 101099

Contents lists available at ScienceDirect

e-Prime - Advances in Electrical Engineering, Electronics and Energy

journal homepage: www.elsevier.com/locate/prime

Integrated techno-economic optimization and metaheuristic benchmarking of grid-connected hybrid renewable energy systems using real-world load and climate data

Aykut Fatih Güven [a], Onur Özdal Mengi [b], Mohit Bajaj [c,d,e,*], Ahmad Taher Azar [f,g], Walid El-Shafai [f,g,h]

[a] Department of Electrical and Electronics Engineering, Yalova University, Yalova, Turkey
[b] Department of Electrical and Electronics Engineering, Giresun University, Giresun, Turkey
[c] Department of Electrical Engineering, Graphic Era (Deemed to be University), Dehradun 248002, India
[d] Hourani Center for Applied Scientific Research, Al-Ahliyya Amman University, Amman, Jordan
[e] Graphic Era Hill University, Dehradun, 248002, India
[f] College of Computer and Information Sciences, Prince Sultan University, Riyadh, Saudi Arabia
[g] Automated Systems and Computing Lab (ASCL), Prince Sultan University, Riyadh 11586, Saudi Arabia
[h] Department of Electronics and Electrical Communications Engineering, Faculty of Electronic Engineering, Menoufia University, Menouf 32952, Egypt

ARTICLE INFO

Keywords:
Battery storage
Diesel generator
Grid-connected system
Hybrid renewable energy system
Metaheuristic algorithms
Microgrid optimization
Photovoltaic-wind integration
Techno-economic analysis

ABSTRACT

This study proposes an integrated optimization framework for the techno-economic sizing and performance evaluation of a grid-connected hybrid renewable energy system (HRES) comprising photovoltaic (PV) panels, wind turbines (WT), battery storage (BTS), and a diesel generator (DG). A real-world case study is conducted on a university campus in Turkey using high-resolution hourly meteorological and load data over a full year (8760 h). The objective is to minimize the annualized cost of the system (ACS), levelized cost of energy (LCOE), and total net present cost (TNPC), while ensuring high reliability through a constraint on the loss of power supply probability (LPSP) at 0.5 %. The decision variables include the optimal capacities of PV, WT, DG, BT, and inverter components, bounded by technical, economic, and operational constraints, including a minimum renewable energy fraction (REF) requirement. The system's energy production, storage, and grid interactions are modeled using detailed mathematical formulations. Optimization is performed using the Moth-Flame Optimization Algorithm (MFOA) and benchmarked against the Whale Optimization Algorithm (WOA), Flower Pollination Algorithm (FPA), and Genetic Algorithm (GA). Simulation results identify the PV/WT/BT configuration as the most cost-effective and reliable, achieving an LCOE of \$0.1342/kWh, a TNPC of \$3.2542 $\times$ 10^6, and an ACS of \$2.9214 $\times$ 10^5. These values reflect a 33 % cost reduction compared to the off-grid configuration. Additionally, the system enables annual grid electricity purchases of up to 4.4086 $\times$ 10^5 kWh and sales of up to 1.2114 $\times$ 10^6 kWh. Notably, the achieved LCOE is significantly lower than the prevailing commercial grid tariff of \$0.35/kWh in Turkey, demonstrating the financial competitiveness of the proposed system for institutional and commercial users. In terms of algorithmic performance, MFOA outperforms the other methods by delivering the fastest convergence, highest optimization stability, and a fully renewable solution (REF = 100 %) without DG operation. This solution achieves an LCOE of \$0.1443/kWh and a TNPC of \$3.5085 $\times$ 10^6, which is slightly higher than the absolute minimum cost but demonstrates the ability to reach 100 % renewable penetration without diesel usage. The system also reports the shortest execution time (336.5 s), confirming its suitability for real-time or iterative design tasks. Overall, the proposed HRES configuration offers a technically feasible, economically advantageous, and environmentally sustainable solution for campus electrification and broader smart grid applications, and serves as a replicable decision-support model for renewable energy planning in regions with high electricity tariffs.

* Corresponding author.
E-mail addresses: afatih.guven@yalova.edu.tr (A.F. Güven), onur.ozdal.mengi@giresun.edu.tr (O.Ö. Mengi), thebestbajaj@gmail.com (M. Bajaj), aazar@psu.edu.sa (A.T. Azar), welshafai@psu.edu.sa, eng.waled.elshafai@gmail.com (W. El-Shafai).

https://doi.org/10.1016/j.prime.2025.101099
Received 13 June 2025; Received in revised form 17 August 2025; Accepted 26 August 2025
Available online 28 August 2025

Nomenclature

Acronyms

ACS	Annual cost of the system
BT	Battery
CRF	Capital recovery factor
C_{grid}	Cost of purchasing power from grid
DG	Diesel generator
DOD	Depth of discharge
FPA	Flower Pollination Algorithm
GA	Genetic Algorithm
HOMER	Hybrid optimization model for electric renewables
HRES	Hybrid Renewable Energy System
LCOE	Levelized cost of energy
LPSP	Loss of power supply probability
MFOA	Moth-Flame Optimization Algorithm
OFS	Objective function of the system
PV	Photovoltaic panel
REF	Renewable energy fraction
RE	Renewable energy
RESs	Renewable energy resources
R_{grid}	Revenue from selling energy to grid
TGE	Total gas emission
TNPC	Total net present cost
WOA	Whale Optimization Algorithm
WT	Wind Turbine

Symbols

$P_{WT}(t)$	The power output of the wind turbine generator
$P_{PV}(t)$	Power generation by photovoltaic panel
$P_L(t)$	Load energy demand at time t
η_{Inv}	Inverter efficiency
$\eta_{\_bat}$	Battery efficiency
$P_{ch}\ (t)$	Power available for battery charging
$E_{ch}(t)$	Energy loaded into the battery
$P_{distch}(t)$	Power to be discharged from battery
$E_{distch}(t)$	Energy discharged from the battery
$E_{b_{min}}$	Energy stored in the battery (minimum)
$E_{b_{max}}$	Energy stored in the battery (maximum)
$E_b(t)$	Energy stored in the battery at time t
$E_{dump}(t)$	Dump Energy
$DG\_hr(t)$	Diesel generator is operational at the specified time
DG_P	Energy output from the diesel generator
SOC_{min}	Lowest battery charge level
SOC_{max}	Highest permissible battery charge level
O&M	Operation and maintenance cost
$E_{grid\_p}(t)$	Energy purchased from grid at time t
$E_{grid\_s}(t)$	Energy sold to grid at time t
E_{served}	Primary load served (kWh/year).
KT	Temperature coefficient of the maximum power for mono and polycrystalline silicon.
t	Time
h	Hours

1. Introduction

Over the past few years, the industry's growth and rising standards of living have significantly increased the energy demand. In the global sense, this rise in energy demand has alarmed many nations, and has unavoidably accelerated the transition to renewable energy resources (RESs). In this context, energy production and conversion into usable forms have always been the goals worldwide. The evolution of clean and sustainable energy resources is currently being pushed by issues such as the depletion of fossil fuel reserves, hazards of nuclear energy use, and pollution in the environment [1]. Domestic RESs are crucial for lowering reliance on foreign energy imports because they are environmentally friendly and sustainable [2]. In terms of avoiding the generation of gaseous or liquid waste, the use of RESs has a significant advantage over conventional energy resources. Viable and environmentally friendly options for supplying electricity to remote or inaccessible locations include power systems based on wind and solar energy [3]. Additionally, by integrating battery storage (BTS) or a diesel generator(DG), an effective power management and distribution strategy can increase the efficiency of renewable-energy-based power supplies. Photovoltaic (PV) components are among the most popular renewable energy technologies owing to ongoing technological advancements and decreases. PV technology is simple to install and requires little upkeep; however, because solar radiation is unpredictable and climate-dependent and varies greatly over the course of a day or an hour, it must be supplemented with grid connectivity, energy storage, or other energy resources [4]. However, effectively managing multiple renewable energy sources integrated within hybrid systems remains a critical challenge, necessitating advanced optimization and control techniques [5].. The energy management, cost-effectiveness, and environmental effects of these systems must be investigated in depth. While increasing the reliability of a PV/wind turbine (WT)/DG system with a grid connection has the benefit of producing revenues by supplying surplus energy to the connected grid, the economic performance of grid-connected PV, WT, and DG systems can be significantly impacted by the implementation of recently developed electricity tariffs. Therefore, extensive research covering all seasonal variations and different tariff structures is essential to ensure practical applicability and economic sustainability of these hybrid systems.

PV, WT, and battery (BT) components must be of the right size when a grid-connected battery-storage PV/WT system is designed first. The use of intelligent optimization techniques established upon a robust rule-based scheme for energy management that coordinates the power flow is necessary to achieve an ideal system component sizing arrangement to cover the load demand. This process can provide maximum reliability while minimizing costs. Here, an optimization problem that considers the sizing of PV, WT, DG, and BT components as well as specific technical and financial constraints should be considered.

A thorough evaluation of PV/WT/DG/BT system optimization in both off-grid and grid-connected systems was conducted in this study. Table 1 demonstrates that despite exhaustive research in this field, there is still a gap in the literature in terms of the comparisons of grid-connected and off-grid operations when factors such as component cost caps, tariff structures, Renewable Energy Fraction (REF), and desired operating reliability are considered.

The novelty of this research lies in the following three aspects:

- Developing an integrated multi-objective optimization framework that simultaneously addressing techno-economic, reliability, and environmental constraints under detailed hourly meteorological and demand data (8760 h).
- Systematically benchmarking multiple advanced metaheuristic algorithms under identical conditions, providing comprehensive comparative insights.
- Incorporating real-world dynamic electricity tariff structures from Turkey, along with rigorous sensitivity analyses on interest rates, LPSP, and converter efficiency.

Despite the extensive body of research on HRES, a clear gap remains in the unified optimization of grid-connected configurations that account simultaneously for techno-economic performance, operational reliability, and renewable energy integration constraints. Prior studies

Table 1
Review of the literature on current research on HRES systems with various parameters.

System type	Energy resources	Energy storage	Findings	Country	Ref.
Grid-connected	PV/WT	BT	To enhance the COE efficiency, a multi-objective design framework was developed for both independent and grid-connected hybrid PV/WT/BT systems. The optimal configuration of the system was established utilizing the artificial electric field algorithm (AEFA) and subsequently validated through a comparative analysis with PSO and gray wolf optimization (GWO).	Iran	[10]
Grid-connected	PV/WT/FC	H_2	A comparative analysis has recently been conducted aiming to achieve cost-effective energy production. This analysis includes a modified seagull optimization technique, the original seagull optimization algorithm (SOA), and a customized version of the farmland fertility algorithm (MFFA). Furthermore, the excess generated energy is integrated into the primary electricity distribution grid, and the system maintains its commitment to zero emissions by harnessing clean energy sources.	China	[11]
Stand-Alone	PV/WT/FC	H_2	System minimization was carried out using a modified version of a novel metaheuristic algorithm known as Improved African vulture optimization (IAVO). Better minimization with higher consistency was achieved for total net present cost (TNPC) using this algorithm.	Iran	[12]
Stand-Alone	PW/WT/DG	BT	For optimizing the HRES, its COE and loss of power supply probability (LPSP) were considered. Techniques like Salp Swarm Algorithm (SSA), grey wolf optimizer (GWO), and improved grey wolf optimizer (IGWO) were implemented, and IGWO showed superior performance.	Saudi Arabia	[13]
Grid -connected	PV	BT	The desired minimum emission and cost of energy (COE) were determined using the HOMER software.	Saudi Arabia	[14]
Grid-connected	PV	BT	A new sizing methodology was presented for PV systems on a grid, each employing diverse battery technologies. In a techno-economic comparison across five battery types, the PV system integrated with a nickel-iron battery outperformed the rest in conditions with high main fault frequencies.	Egypt	[15]
Stand-alone	PV/WT/FC/ DG	BT, H_2	Using HOMER software, the energy production of Koh Samui, a well-known island that caters to tourists and is located in the Gulf of Thailand, was examined in the context of energy independence and renewable energy-based electricity generation.	Thailand	[16]
Grid-connected /Stand-alone	PV/BG/ BMG	BT	The study contrasted stand-alone with grid-connected configurations. Leveraging the Aquila optimization technique, the grid-connected system outperformed HS and PSO, boasting the least net present cost (NPC) and reduced energy cost.	India	[17]
Grid-connected	PV	–	The ideal PV system size for meeting the load requirements of a public building and the electric vehicles used by its occupants is presented. While both single and multiple optimization processes were carried out, the carbon footprint, amount of grid power purchased, and COE decreased.	France	[18]
Grid-connected	PV/WT	–	Optimized using hybrid methods combining PSO, GA, GWO, ABC, and Marquardt Gradient Descent (MGD), achieving an annual energy production above 5000 kWh and minimum LCOE of 0.0662 $/kWh, with an optimal REF $\geq$80 %.	Morocco	[19]
Grid-connected	PV/WT	BT	Systematic literature review identifying critical gaps in optimization strategies, energy storage integration, and economic feasibility analyses. Emphasized need for advanced methodologies to ensure reliable integration of HRES into national power grids.	Brazil	[20]
Grid-connected	PV/WT	BT	Probabilistic model using Monte Carlo simulations and dynamic parameter Bald Eagle Search (DP-BES) algorithm, achieving maximum cost reduction (41 %) compared to standalone PV (33 %) or wind systems (25 %). Reliability ensured via LPSP.	Iran	[21]
Stand-alone	PV/WT	BT	Proposed a novel Caracal Optimization Algorithm (CAO) demonstrating superior performance compared to GWO, Whale Optimization Algorithm (WOA), zebra optimization algorithm (ZOA), and PSO. Achieved the lowest LCOE (0.1069 $/kWh), lowest net present cost (NPC), and superior solution convergence for off-grid PV/ wind/battery systems.	Cameroon	[22]
Grid-connected	PV/WT/DG	BT	Comparative techno-economic analysis of incentive-based demand response policies using Circle Search Algorithm (CSA). Reduced generation cost from $25,463 to $24,969 (IBDR1) and $24,899 (IBDR2), with significant customer and DISCOM benefits.	India, South Africa	[23]
Grid-connected	PV	–	Developed a solar power plant electricity supply chain model optimized using Particle Swarm Optimization (PSO) algorithm under uncertainties (electricity demand, solar radiation). Determined optimal PV plant capacities to minimize conventional gas power plant consumption and emissions.	Iran	[24]
Grid-connected	PV	–	Implemented forecasting frameworks (ARIMA model) to enhance Virtual Power Plant (VPP) performance. Achieved high prediction accuracy for PV generation (MAE:1.219, R^2:0.899 in summer), facilitating optimized energy scheduling, demand response, and integration of renewables.	North Macedonia	[25]
Stand-alone	PV/WT	BT	Optimized off-grid PV/WT/BT system sizing using Black-Winged Kite Algorithm (BKA). Achieved the lowest total annual cost (TAC: $7105.23) and LCOE of $0.1874/ kWh, demonstrating superior results compared to HHO, SCA, WSO, and AOA algorithms, while ensuring LPSP $\leq$5 %.	India (Puri, Odisha)	[26]
Grid-connected	PV	–	Techno-economic analysis conducted for optimal tilt-angle configurations in PV systems across diverse climates in Iran. Optimal annual tilt angle achieved superior economic performance with payback periods ranging from 3 to 6 years and enhanced CO_2 reduction capabilities.	Iran	[27]
Grid-connected/ Stand-alone	PV/WT/ BG/DG	BT, Hydrogen, Pumped Hydro	Comprehensive review covering techno-economic and environmental assessments of ESS-integrated hybrid renewable energy systems (HRES). Analyzed various ESS types and optimization techniques, highlighting significant research gaps in cost-effective sizing, operational management, and hybrid ESS integration.	Bangladesh, Malaysia, Australia	[28]

(*continued on next page*)

Table 1 (*continued*)

System type	Energy resources	Energy storage	Findings	Country	Ref.
Grid-connected	PV	–	Developed novel hybrid machine learning approaches (series and parallel models combining Artificial Neural Networks and Boosting Trees) for predicting greenhouse energy consumption and PV energy production. Models demonstrated effective performance (10 % < nRMSE < 30 %), especially under dynamic external temperature and solar radiation conditions.	Morocco	[29]
Grid-connected	PV/WT	BT	Introduced Transactive Energy Management (TEM) using the Slime Mould Algorithm (SMA) for efficient scheduling and storage optimization in renewable energy-based microgrids. Achieved 20–48 % cost savings through optimal BT charge/discharge cycles and reduced emissions by 25–38 %, significantly outperforming traditional optimization methods.	South Africa	[30]

have largely focused either on off-grid scenarios, simplified grid interactions, or limited comparative analysis of optimization methods. Moreover, most existing works overlook the dynamic interplay between grid purchase/sale tariffs, energy storage behavior, and sizing strategies under varying reliability thresholds. Although several metaheuristic algorithms have been employed individually in HRES design, a rigorous comparative evaluation of their effectiveness under identical conditions is seldom addressed. Therefore, the problem to be addressed in this study involves the development of an integrated multi-objective optimization framework that accurately models real-world meteorological and demand conditions, incorporates component and grid constraints, and systematically benchmarks multiple advanced metaheuristic algorithms to identify the most cost-effective and reliable system configuration for grid-connected HRES applications.

Despite substantial contributions by previous studies, several critical aspects still require further investigation. Particularly, most existing studies either neglect dynamic tariff structures, lack detailed sensitivity analyses, or do not sufficiently address the interplay between economic parameters and REF. Additionally, conventional and metaheuristic optimization methods have limitations in terms of convergence, computational time, or getting stuck in local optima [31–36].

Researchers in the cited literature have reported conventional and meta-heuristic optimization techniques as software tools for analyzing performance. Software tools have considerable drawbacks and take longer to compute than current optimization methods. To circumvent the issue that conventional techniques are frequently stuck at local minima, researchers have combined conventional and evolutionary algorithms to determine the optimal sizes in hybrid systems [31–36].

Several relevant studies have attempted to address these gaps with varying approaches: Maleki et al. [6] investigated how grid purchase and sale tariffs affected a hybrid energy system made up of grid-connected PV, wind, and fuel cell components. It has been demonstrated that this is a better option than grid prices. Seasonal analyses could not be performed because their results were based on daily load data, considering the minimum daily operating and maintenance costs. Samy et al. [7] used grid-connected HRES including the components of WT, PV, and FC to cover the electricity load requirements of a resort for tourists in Hurghada, Egypt. They evaluated the cost of buying electrical energy and the revenue from selling it to the grid. Particle swarm optimization (PSO), hybrid firefly optimization, and harmony search optimization techniques were used to reduce the net present cost of the proposed system. The results additionally demonstrated that the system collected 4 GW from the grid and sold 3 GW to the grid. Recently, Güven et al. [8] used HOMER, Ant Colony Optimizer, and Jaya algorithms for optimal sizing of an off-grid PV/WT/DG/BT energy system. Despite obtaining 1.8431×10^6 kWh of excess energy, grid sales were not deemed appropriate. Güven and Samy [9] used Hybrid Firefly Genetic Algorithm (HFGA), Genetic Algorithm, Cuckoo Search Algorithm, and Sine-Cosine Algorithm for a techno-economic evaluation of off-grid WT, PV, biomass gasifier (BG), and fuel cell (FC) systems including hydrogen storage. The system produced 8.0280×10^5 kWh excess energy, without considering grid sale opportunities.

In line with these identified limitations, the following objectives are formulated to guide the scope of this study:

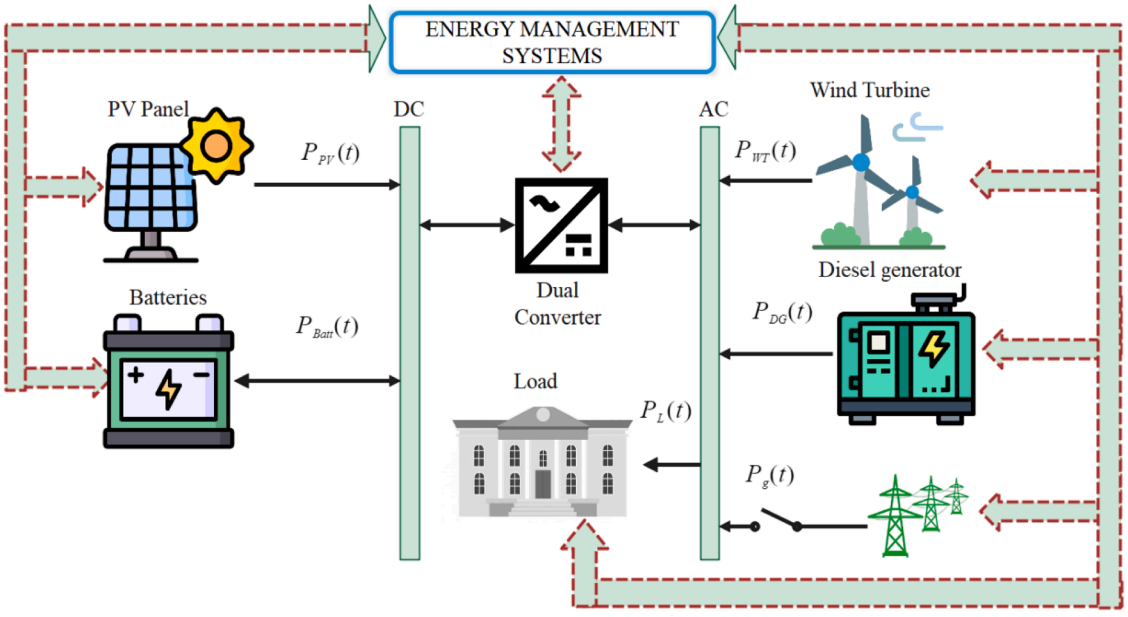

Fig. 1. Grid-connected PV/WT/DG/ BT model proposed by the researchers for the research area.

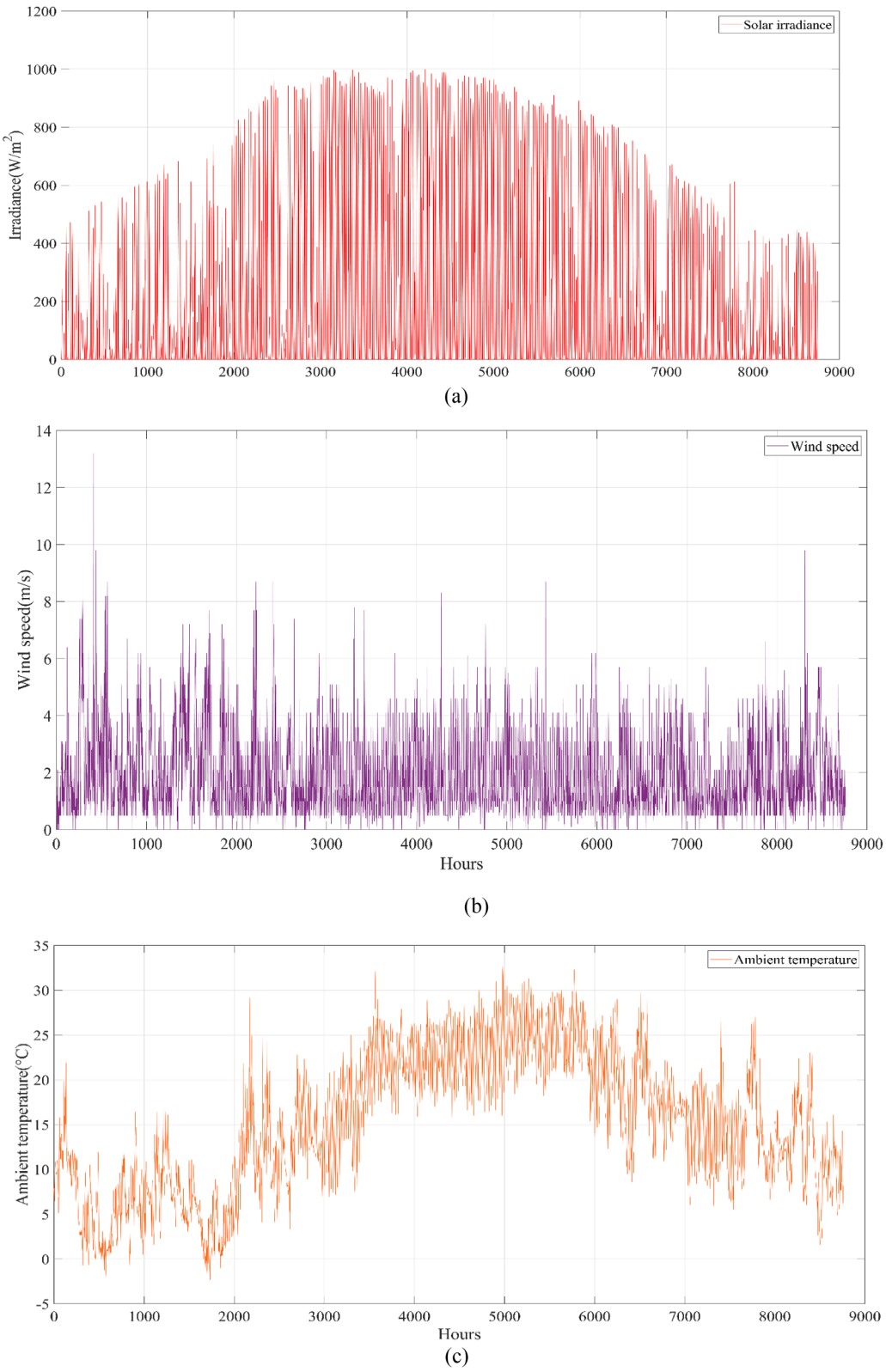

Fig. 2. The weather patterns of the study area. (a) solar radiation (W/m^2), (b) wind speed (m/s), (c) ambient air temperature (°C).

- Identifying optimal configurations and sizing parameters for a grid-connected HRES including PV, WT, DG, and BT.
- Performing a comprehensive techno-economic-environmental assessment using real-world hourly load and meteorological data.
- Evaluating the reliability and sensitivity of proposed systems to varying parameters including LPSP, economic factors, and converter efficiency.

The main goal of this study is to identify the ideal parameters for a grid-connected HRES, taking into account both financial and

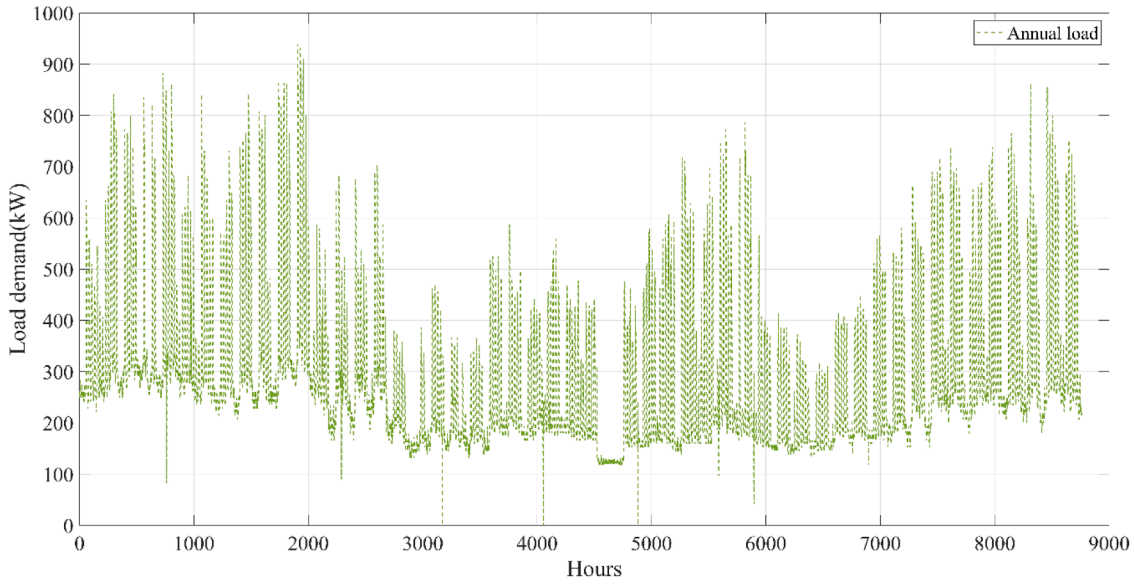

Fig. 3. Annual load profile for the campus.

environmental considerations, and to compare the results of the optimization process using metaheuristic algorithms. In this study, the levelized cost of energy (LCOE), TNPC, and annual cost of the system (ACS) were identified as objective functions of the proposed HRES. Real-world weather data and load demand values of 8760 h were used for optimization (one year). Examining the effect of the system component reliability on the proposed design is another goal of this study. However, optimal system configuration still poses a challenge due to varying site-specific conditions, component interactions, and dynamic market structures.. New technologies and approaches are required to reduce or eliminate the current emission rates. Global warming can be reduced in the future with HRESs produced using RES components.

The objectives for the techno-economic-environmental analysis of the HRES, based on the intended contribution to the literature, are outlined as follows:

- The proposed microgrid sizing method is based on a grid-connected PV/WT/DG/BT configuration that simulates real-world microgrid behavior. When RESs produce more energy than needed, the excess is fed into the grid.A meta-heuristic algorithm grounded in set rules was implemented to devise an energy-control approach for the microgrid, drawing insights from the simulation model depicted in Fig. 1. This specific EMS manages the flow and distribution hierarchies among the diverse microgrid elements.
- Modeling systems and energy management techniques yield diverse results. A primary phase of this research involves utilizing mathematical equations in a MATLAB environment for system management. Consequently, varying input data such as weather conditions, energy consumption, and types of system components can be easily modified.
- The algorithms proposed in this study to determine the minimum ACS, optimal HRES sizes, and other energy parameters demonstrate the ability of this study to address this issue.
- Energy production and numerous related cost calculations were subjected to a sensitivity analysis of changes in LPSP values, interest rates, and converter efficiency.
- The analyses in this study will aid researchers in selecting the best technique for their specific HRES design optimization problems. The remainder of this paper is organized as follows.

Research Questions

In light of the identified research gap, this study is guided by the following research questions:

- RQ1: What is the optimal sizing configuration of a grid-connected PV/WT/DG/BT hybrid renewable energy system under real-world meteorological and load conditions?
- RQ2: How do different metaheuristic algorithms compare in terms of cost minimization, reliability enhancement, and energy performance when applied to identical hybrid system configurations?
- RQ3: What are the techno-economic and environmental impacts of dynamic grid tariff structures, interest rate variations, and energy storage parameters on system behavior?

The remainder of this paper is structured into five sections: Section 2 presents the modeling of the hybrid energy generation system and its renewable components. Section 3 describes the methodology, system configuration, load profile characteristics, and optimization strategies. Section 4 presents the simulation results and discussions. Finally, Section 5 concludes the paper and offers directions for future research.

2. Mathematical representation of hybrid renewable energy system

Fig. 1 presents a schematic overview of the HRES, encompassing the load associated with the university's main campus, connections to the grid, and elements such as PV, WT, DG, and BT. In situations where the PV yield falls short, the BT utilizes surplus energy to fulfill the demand. To avoid overcharging and overdischarging of the BT, a charge controller was employed. In this section, the mathematical representations of the system's components, definitions of the objective functions, and explanations of the system's energy management scheme are presented. The COE produced by the system was determined based on the lifespan of the project and all its components, using the discounted cash flow analysis method. The lifetimes of the WT, BT, and PV components were assumed to be 15, 20, and 25 years, respectively. The projected lifespan of the system is assumed to be 20 years. To ensure that the calculations were accurate, interest rates (Ir) were considered as a financial criterion were taken into consideration. The proposed grid-connected PV, WT, DG, and BT systems are shown in Fig. 1.

2.1. Meteorological and electrical load data

The proposed Hybrid Renewable Energy System (HRES) was

modeled for implementation at a university campus in Turkey, geographically located at 40°39.2′N latitude and 29°13.2′E longitude. Meteorological data were acquired from the Turkish State Meteorological Service and included hourly records of solar irradiance, wind speed, and ambient air temperature. The hourly electrical load profile was obtained from the university's Energy Management Unit, which continuously records real-time consumption data using a centralized monitoring system. All load measurements used in the study were directly measured and extracted from the institution's internal data infrastructure. These data, along with the hourly electrical load profile, were utilized to construct a comprehensive annual energy and environmental profile for the study site. Fig. 2 illustrates the temporal distribution of key meteorological parameters—namely, wind speed measured at 10 m above ground level, ambient temperature, and solar radiation—recorded hourly over a one-year period (8760 h). The average daily electricity demand on the campus was calculated to be approximately 6947.06 kWh. The observed maximum and minimum hourly load values during the year were 938.50 kW and 289.46 kW, respectively. The corresponding hourly load demand profile for the case study is presented in Fig. 3. All input data were stored in a modular structure within the MATLAB simulation environment. This configuration allows the proposed framework to be readily adapted for other geographical locations by simply updating the input datasets with new hourly meteorological and load data. Thus, the model can be flexibly applied to different regions for site-specific HRES planning.

2.2. PV component modeling

To accurately model the performance of a PV component, it is essential to consider its peak power output behavior. The ability of the PV module to produce high-quality power can be influenced by a number of factors. Some of these factors include the amount of solar radiation that reaches the surface, fixed solar panel orientation, properties of the PV modules, and ambient air temperature at the specified time. Eq. (1), a streamlined model that accounts for the solar radiation and ambient air temperature values, was employed in this study to calculate the output power of the PV generator over the course of a year [37].

$$P_{pv_{out}}(t) = P_{(PV_{rated})} \times \frac{G_{(t)}}{G_{t-STC}} \times \ [1 + \alpha_t (T_C(t) - T_{C-STC} \tag{1}$$

Here, $P_{pv_{out}}(t)$ is the PV module's output power (W), $G_{(t)}$ is the solar radiation value (W/m^2), $P_{(PV_{rated})}$ is the rated power value in standard test conditions (STC) for PV (W), G_{t-STC} is the solar radiation value in STC ($G_{t-STC} = 1000\ W/m^2$), α_t is the temperature defined by -3.7×10^{-3}(1/°C), $T_{C-\mathrm{STC}}$ is the cell temperature in STC ($T_{C-\mathrm{STC}} = 25$ °C), and T_{amb} is the ambient air temperature (°C). The cell temperature $T_C(t)$ was calculated using Eq. (2) [38].

$$T_C(t) = T_{amb}(t) + [0.0256\ x\ G_t(t)] \tag{2}$$

2.3. WT component modeling

Wind is one of the most valuable and promising resources for a HRES when properly modeled and managed. Hub height, surface topography, and turbine speed characteristics affect the wind output differently. These elements influence the energy production of the WT generator at a given site. The power output from the wind was significantly influenced by the height of the turbine above the reference ground. The height adjustment equation can be used to adjust the appropriate height during the assembly. Eq. (3) can be used to determine the power output of the WT [39]:

$$P_{WT} = \begin{cases} 0 & v(t) \le v_{cut-in} \\ P_r \dfrac{v(t) - v_{cut-in}}{v_r - v_{cut-out}} & v_{cut-in} < v_r \\ P_r & v_r < v(t) < v_{cut-out} \end{cases} \tag{3}$$

P_r is the WT nominal power (kW), $v(t)$ is the wind speed (m/s), $v_{cut-out}$ is the low shear speed of WT (m/s), v_r is the WT nominal speed (m/s), and v_{cut-in} is the high shear speed of WT (m/s).

In Eq. (4), the wind speed based on the reference altitude and the influence of the power law constant are the factors that determine the wind speed at a consistent altitude.

$$V_t = V_m * \left(\frac{H_t}{\mathrm{H_m}}\right)^{a_h} \tag{4}$$

In Eq. (4), $\mathrm{H_m}$ is the WT reference height (m), H_t is the WT hub height (m), V_m is the wind speed at the WT hub height (m/s), V_t is the speed at the reference height (m/s), and a_h is the exponential power law value, typically taken as 1/7.

2.4. BT component modeling

Because the outputs of PV cells and WTs are naturally stochastic, modeling the BT component is crucial for ensuring that the load demand is met. The current state of charge (SOC) is the primary deciding factor for managing BT overcharge and overdischarge. When the hybrid system generates a surplus of power or when the load demand is low, the BT can be overcharged. The control system steps in and stops charging when BT reaches the maximum value of E_{BT_max}. Here, the control system reduces the load when the E_{BT_min} value is reached to prevent the shortening of the BT life. The output power and energy demand determine the BT state at any given moment. By balancing the load demand and supply, the BT plays a significant role in the energy management process of the system. BT is entirely reliant on its previous SOC at any given hour. In this case, t ($t - 1$) hours are used to express the energy production, consumption, and changes in the BT's SOC. When other resources, such as WT, DG, and PV, generate more energy than is needed by the load, surplus energy must be used to charge batteries and store it in BT banks. Eq. (5) can be used to express the current capacity of the BT bank at time h [40].

$$\mathrm{E_{BT}(t)} = \mathrm{E_{BT}}(t-1)(1-\sigma) + \left[\mathrm{E_{WT}(t)} + E_{\mathrm{PV}}(\mathrm{t}) - \frac{\mathrm{E_{Load}(t)}}{\eta_{\mathrm{Inv}}}\right]\eta_{\mathrm{BC}},\ \text{Charge} \tag{5}$$

Energy is supplied by the BT and released in the process in the opposite scenario, that is, when the total power generated by the other resources is not sufficient to meet the load demand. Accordingly, Eq. (6) can be used to express the usable capacity of the BT component at hour t during the discharge process.

$$\mathrm{E_{BT}(t)} = \mathrm{E_{BT}}(t-1)(1-\sigma) + \left[\frac{\mathrm{E_{Load}(t)}}{\eta_{\mathrm{Inv}}} - (\mathrm{E_{WT}(t)} + E_{\mathrm{PV}}(\mathrm{t}))\right]\eta_{\mathrm{BD}}, \text{Discharge} \tag{6}$$

$\mathrm{E_{BT}(t)}$ represents the BT's available capacity at hour t (kWh), $\mathrm{E_{BT}}(t-1)$ represents the BT's available capacity at an hour (t-1) (kWh), $\mathrm{E_{Load}}$ stands for the load demand at hour t (kWh), $\mathrm{E_{WT}}$ represents the energy production of the WT at hour t (kWh), σ represents the BT's rate of self-discharge, $\mathrm{E_{PV}}$ represents the energy production of the PV-module at hour t (kWh), η_{BC} represents the efficiency of BT charging, η_{BD} represents efficiency of BT discharging, and η_{Inv} represents the efficiency of the inverter. The BT charging efficiency values, denoted by η_{BC} and η_{BD} in Eqs. (5) and (6),respectively, varied depending on the charging current at different stages. A BT must exhibit different charging and discharging efficiencies. In this study, it was assumed that the charging efficiency would always be 90 %.

Batteries are used to store the surplus energy generated by renewable resources. However, BT size is a limiting factor. A large amount of en-

ergy cannot be stored in any BT. Excess power must be discharged if the BT is fully charged. The capacity of BT is referred to as the depth of discharge (DOD). Because of their chemical composition, most batteries must be charged, and if a BT is constantly used at 100 % charge, its lifespan will be shortened. The BT capacity increases with an increase in the DOD value. The SOC and DOD had a negative relationship. The maximum permitted DOD value is presented as a percentage. In this study, this value was assumed to be 80 %. Eq. (7) was used to calculate the minimum BT capacity [41]:

$$E_{BT\_min} = (1 - DOD)E_{BT\_max} \tag{7}$$

Here, the DOD maximum permissible depth of BT discharge (%), E_{Batt_max} and E_{Batt_min} are the maximum and minimum capacities of the BT, respectively.

One of the most crucial components of optimization calculations is the BT capacity, which determines the rate at which BT will be charged. When the desired time in hours is multiplied by the current used to discharge the BT, the result is the BT's capacity, which is measured in ampere-hours (Ah) [42]. As measured in kilowatt-hours (KWh), the capacity is the amount of electricity that can be stored in the BT (kWh). The BT power determines the amount of electricity it can produce and is measured in (kW). Therefore, high-power and low-capacity BT can be powered by other components of the system more quickly than high-capacity and low-power BT [43]. Eq. (8) expresses the BT capacity constraint for any given time.

The ratio of the energy output to the energy input for a BT is known as round-trip efficiency. The round-trip efficiency is 9 kWh/10 kWh or 90 % if the BT input is 10 kWh and its output is 9 kWh. Therefore, for cost-effective selection of the BT component, its round-trip efficiency must be high [44].

$$E_{BT\_min} \leq E_{BT}(t) \leq E_{BT\_max} \tag{8}$$

2.5. DG component modeling

In the HRES proposed in this study, DG was used to compensate for insufficiencies in the power generated by the BT and RESs. While a DG's maintenance costs are influenced by the amount of time its engine is running and the load it supports, its operating costs are related to fuel consumption. Although the typical DG fuel consumption characteristic curve is quadratic in nature, a linear function is used as a simplified model in Eq. (9) [45].

$$q(t) = a_{dg}P_{DG}(t) + b_{dg}P_r \tag{9}$$

where, $P_{DG}(t)$ represents the power output of DG at hour t (kW), $q(t)$ represents the consumption of fuel (L/h), P_r represents the average DG power, and a_{dg} and b_{dg} (L/kW) are constants that represent the parameters of standard fuel consumption, which were 0.246 and 0.08415, respectively.

2.6. Inverter

A converter, which is an electronic device, can operate in two ways. A converter that converts direct current (DC) to alternating current (AC) is called an inverter. When it converted to DC, it is called a rectifier [46]. A converter can also be bidirectional [47]. Owing to its capacity to serve as both an inverter and rectifier simultaneously, a bidirectional converter is a crucial component and is employed in hybrid systems. By converting the energy generated by the PV panels and the energy stored in the BT, both of which are connected to the DC busbar, into an AC, power is supplied to the electrical load. In this instance, it functions as an inverter. Additionally, when it converts the energy generated by the DG and WT components, both of which are connected to the AC busbar, it functions as a rectifier to charge the BT [48].

The input power P_{inv} of the inverter is calculated in this study using Eq. (10), where the size of the inverter is determined based on the maximum load demand [49].

$$P_{inv}(t) = P_L(t)/\eta_{inv} \tag{10}$$

Here, $P_L(t)$ and η_{inv} represent load power and inverter efficiency, respectively.

Table 2
Technical and economic characteristics of HRES components.

Components	Parameters	Value	Unit
A. Solar Panel	Capacity of solar panel	0.345	kW
	Temperature coefficient of solar panel	−0.390	
	Productivity	17.8	%
	Operating temperature	44	°C
	lifespan of solar panel	20	Years
	Replacement cost of solar panel	650	$/kW
	O&M cost of solar panel	50	$/Year
	Capital cost	650	$/kW
B. Wind Turbine	Rated power of turbine	1	kW
	Hub height of turbine	17	m
	O&M cost of wind turbine	200	$/Year
	Replacement cost of wind turbine	2000	$/kW
	Cost of capital	2000	$/kW
	Lifespan of wind turbine generator	20	Year
C. Battery	Rated voltage of battery	600	V
	Rated capacity of battery	100	kWh
	Maximum capacity of battery	167	Ah
	Round-trip efficiency of battery	90	%
	Maximum battery charging current	167	A
	Minimum battery charge status	20	%
	Maximum battery discharge current	500	A
	Lifespan of battery bank	10	Year
	Replacement cost of battery	550.00	$/kW
	Capital cost of battery	550.00	$/kW
D. Diesel Generator	Capacity of diesel generator	1000	kW
	Capital cost of diesel generator	175	$/kW
	O&M cost of diesel generator	30	$/kWh
	Replacement cost of diesel generator	175	$/kW
	Fuel price of diesel generator	1	$/L
	Lifespan of diesel generator	10	Year
E. Inverter	Capacity of inverter	1	kW
	Replacement cost of inverter	300	$/kW
	Capital cost of inverter	300	$/kW
	O&M cost of inverter	50	$/Year
	Productivity of inverter	95	%
	Lifespan of inverter	15	Year
F. Economic Parameters	Interest rate dynamics in Turkey	19	%
	Inflationary trends in Turkey	16.59	%
	Discount rate benchmarks in Turkey	8	%
	Operational duration of HRES	20	Year

2.7. Grid modeling

The electrical grid functions as an integrated infrastructure that connects various energy sources, facilitating the generation, distribution, and temporary storage of electricity. Within the proposed system architecture, energy can be imported from the grid to supplement the load demand when the energy output from PV, WT, and B units is insufficient. Additionally, the DG operates as a standby unit to ensure supply continuity under critical shortages.

The revenue generated from exporting excess energy to the grid is calculated using Eq. (11) [50]:

$$\mathrm{R_{grid}} = \sum_{t=1}^{8760} \mathrm{r_{feed\_in}}.E_{grid\_s}(t) \tag{11}$$

where r_{feed_in} denotes the feed-in tariff rate, specified in this study as $0.01/kWh based on actual market values. Conversely, the cost associated with grid power procurement is computed using Eq. (12):

$$C_{grid} = C_p \sum_{t=1}^{8760} E_{grid\_p}(t) \quad (12)$$

Here, C_p represents the cost of purchasing 1 kWh of electricity from the grid, estimated at $0.25/kWh for the case study location. This value was obtained from the University's Department of Construction Works to reflect realistic pricing data. Furthermore, grid availability (GA) is an essential metric for evaluating the reliability of grid connectivity and is defined in Eq. (13) as:

$$GA(\%) = \frac{\text{Grid uptime}}{\text{Grid downtime}} x100 \quad (13)$$

This parameter provides insight into the operational dependability of the grid throughout the simulation horizon.

2.8. Economic parameters

Accurate economic assessment is essential for evaluating the financial feasibility and long-term sustainability of hybrid energy systems. In this study, key economic indicators were established, including a real interest rate of 19 %, an inflation rate of 17 %, and a discount rate of 8 %. The projected operational lifespan of the proposed HRES configuration was assumed to be 20 years, aligning with typical engineering and financial planning horizons.

To ensure realistic modeling, cost estimates for individual system components were obtained directly from equipment manufacturers and integrated into the simulation framework. These values form the foundation of the economic analysis, enabling the computation of lifecycle costs and investment viability. The technical and financial specifications associated with each microgrid component are summarized in Table 2.

2.9. LPSP-based power reliability constraint

The dependability of the microgrid system was assessed according to the LPSP. Owing to the existence of numerous factors, including intermittent solar radiation characteristics, wind speed, and grid downtime, which affect the reliability of the proposed system and its capacity to fully meet the required load at all times, analyzing energy reliability is a crucial step in the system design process. Energy reliability is a parameter that indicates the likelihood that in the event of an insufficient power supply, the hybrid model will be unable to meet the load requirement [51]. LPSP was calculated using Eq. (14).

$$LPSP = \frac{\sum_{t=1}^{8760} P_{deficit}(t)}{\sum_{t=1}^{8760} P_{demand}(t)} \quad (14)$$

Here, $P_{deficit}(t)$ is the power deficit at time t and $P_{demand}(t)$ is the power consumed at time t. The value interval of LPSP is [0,1] [52].

2.10. Renewable fraction (REF)

Several performance indicators have been utilized to evaluate the contribution of RE sources in hybrid power systems. Among these, the REF is a widely adopted metric aimed at quantifying and maximizing the share of renewables, thereby reducing dependence on non-renewable energy sources such as diesel generators. For diesel-based HRES configurations, the REF value is calculated using Eq. (15) [53]:

$$REF(\%) = \left(1 - \frac{\sum_{t=1}^{8760} P_{DG}(t)}{\sum_{t=1}^{8760} P_{PV}(t) + P_{WT}(t)}\right) 100 \quad (15)$$

In this expression, $P_{DG}(t)$, $P_{PV}(t)$, and $P_{WT}(t)$ represent the power outputs of the DG, PV system, and WT at time step ttt, respectively. To enhance the renewable penetration within the system, the denominator of the equation should be maximized while minimizing DG usage.

The REF serves as an optimization objective and is bounded above by 100 %. In practical optimization scenarios, it is treated as a constraint to ensure that the renewable contribution meets or exceeds a predefined target ε_{REF}, as expressed in Eq. (16) [54]:

$$REF(\%) \leq \varepsilon_{REF} \quad (16)$$

This constraint guides the algorithm toward solutions that favor higher shares of renewable energy without violating system reliability or operational constraints.

2.11. Design variables

In this study, the design variables—also referred to as decision variables—comprised the rated capacities of WT, PV, BT, and DG. The operational limits of these variables, in terms of their lower and upper bounds, are defined in Eq. (17):

$$\text{Decision Variables} = \begin{cases} 1\ kW \leq R_{WT} \leq 5000\ kW \\ 1\ kW \leq R_{PV} \leq 5000\ kW \\ 1\ kW \leq R_{BT} \leq 800\ kW \\ 1\ kW \leq R_{DG} \leq 1000\ kW \end{cases} \quad (17)$$

Here, R_{WT}, R_{PV}, R_{BT}, and R_{DG} represent the installed power capacities of the WT, PV array, BT system, and DG, respectively. Establishing appropriate boundary conditions for these variables is inherently problem-specific, and greatly influences the convergence behavior of the applied optimization algorithms. In this context, the bounds were determined through iterative testing and sensitivity analysis, enabling the identification of value ranges that yielded the most favorable and stable optimization outcomes.

3. Objective function

The ACS was designated as the primary objective function for evaluating the performance and economic feasibility of the microgrid configuration. The optimization process aimed to achieve a reliable and uninterrupted power supply while minimizing the overall system cost. Four critical decision variables—WT capacity, PV capacity, BT storage size, and DG capacity—were selected to determine the optimal system configuration. ACS is a widely utilized metric in economic analyses, as it provides a normalized cost representation over the system's lifetime. The configuration yielding the minimum ACS value is considered the most cost-effective solution, provided it adheres to all predefined technical and operational constraints. In addition to ACS, other performance indicators such as LCOE, TNPC, REF, and the capacities of PV, WT, DG, BT, and power converters were incorporated as key decision-making parameters in the optimization model. The mathematical formulation of the ACS objective function is presented in Eq. (18) [55].

$$Objective\ Function = Min(ACS,\ TNPC,\ LCOE)\ \{R_{WT},\ R_{PV},\ R_{BT}, R_{DG}\ \} \quad (18)$$

$$ACS = Min\ (DG_{cost} + \\ + Inverter_{Tcost} + Wind_{cost} + Battery_{cost} + Solar_{cost} + Grid_{cost}) \quad (19)$$

Subject to:

$$SOC_{min} \leq SOC \leq SOC_{max}$$

$$REF > 10\%$$

In this study, the optimization of the HRES was performed using advanced meta-heuristic algorithms, with a population size set to 40 for each algorithm. This choice balances computational efficiency and thorough exploration of the solution space. The system's maximum LPSP was constrained to $LPSP_{max}$==0.5 %, ensuring high reliability in the energy supply. Additionally, the efficiency of the BT system was assumed to be 90 %, which accurately reflects typical performance under real-world conditions.

The optimization process set the maximum capacities as follows: WT

at 5000 kW, PV system at 5000 kW, BTS at 800 kW, and DG at 1000 kW to ensure optimal energy generation and storage. Moreover, the minimum REF was set at 10 % to ensure that a significant portion of the energy comes from renewable sources. Key efficiency parameters were also incorporated into the model, including 95 % for both the converter and inverter efficiencies, addressing the inherent inefficiencies in energy conversion and storage processes.

By incorporating these technical constraints and efficiency parameters, the model achieves a more accurate and realistic representation of the system's operational performance. These assumptions and constraints serve as the foundation for optimizing the system's design, while also accounting for potential uncertainties, such as input variability and the challenges of modeling real-world conditions.

a. **Cost Analysis**

From an economic standpoint, this study conducts a comprehensive assessment of the cost structure associated with the proposed HRES, which comprises PV panels, wind turbines, BTS, diesel generators, and a grid interface. The financial modeling approach adopted in this work integrates a wide spectrum of economic parameters to facilitate a detailed and reliable cost evaluation. Core elements of this model include the initial capital expenditures, periodic operation and maintenance costs, component replacement costs over the system's projected lifetime, salvage values recoverable at the end of operation, and the effect of real interest rates on long-term financial planning.

This rigorous methodology ensures a holistic understanding of the economic performance of HRES configurations. By accounting for the full financial lifecycle—from deployment to decommissioning—the model establishes a solid foundation for computing the system's total annualized cost. Such detailed financial analysis is pivotal in guiding investment decisions and operational planning, ultimately enhancing the economic feasibility and long-term sustainability of hybrid energy projects.

The capital investment associated with the BT subsystem is determined using the following formulation:

$$Battery_{costC} = N_{bat} \times \left[BAT_C \times \left(\frac{ir \times (1+ir)^{PRJ_{LF}}}{(1+ir)^{PRJ_{LF}} - 1} \right) \right] \tag{20}$$

The BT replacement cost is calculated as:

$$Battery_{cost_r} = N_{bat} \times BAT_{C_r} \times \left[\left(\frac{1}{(1+ir)^{Bate_{LF}}} \right) \times \frac{ir \times (1+ir)^{PRJ_{LF}}}{(1+ir)^{PRJ_{LF}} - 1} \right] \tag{21}$$

The BT salvage cost is calculated as follows:

$$Battery_{sal_{cost}} = N_{bat} \times BAT_{C_r} \times \left[\left(\frac{Bate_{sal_f r}}{Bate_{LF}} \right) \times \frac{1}{(1+ir)^{PRJ_{LF}}} \times \frac{ir \times (1+ir)^{PRJ_{LF}}}{(1+ir)^{PRJ_{LF}} - 1} \right] \tag{22}$$

The total BT cost is calculated as follows:

$$Battery_{cost} = Battery_{costC} + Battery_{cost_r} + (N_{bat} \times Bat_{OM}) - Battery_{sal_{cost}} \tag{23}$$

A comprehensive evaluation of BT-related costs within the renewable energy system was conducted using Eqs. (20) through (23), each capturing a distinct financial component. Eq. (20), denoted as $Battery_{costC}$, estimates the total initial capital investment for BTS. This formulation incorporates the number of BT units (N_{bat}), unit cost of each BT (BAT_C), interest rate (ir), and the overall project lifetime (PRJ_{LF}), thereby reflecting both upfront expenditure and its amortization across the system's operational period. Eq. (21), referred to as $Battery_{cost_r}$, quantifies the replacement costs incurred throughout the lifecycle of the project. It introduces variables such as the replacement cost per BT (BAT_{C_r}) and BT lifespan ($Bate_{LF}$) to determine the frequency and financial impact of necessary replacements. Subsequently, Eq. (22) computes the salvage value of the batteries, labeled as $Battery_{sal_{cost}}$, which represents the residual value recoverable at the end of the project duration. This is calculated using the salvage factor ($Bate_{sal_f r}$) and the BT lifetime ($Bate_{LF}$). Lastly, Eq. (23) aggregates all these components—initial capital cost, replacement cost, operational and maintenance expenses ($N_{bat} \times Bat_{OM}$), and the salvage value—to yield the overall BT cost. This multifaceted approach enables a holistic and accurate representation of BT economics within the hybrid energy system.

The formula for computing the capital cost of the wind energy component is as follows:

$$Wind_{cost_c} = N_w \times \left[C_{wr} \times \left(\frac{ir \times (1+ir)^{PRJ_{LF}}}{(1+ir)^{PRJ_{LF}} - 1} \right) \right] \tag{24}$$

The WT replacement cost is calculated as:

$$Wind_{cost_r} = N_w \times \frac{1}{(1+ir)^{Wind_{LF}}} \times \left[C_{wr} \times \left(\frac{ir \times (1+ir)^{PRJ_{LF}}}{(1+ir)^{PRJ_{LF}} - 1} \right) \right] \tag{25}$$

The WT salvage cost is calculated as:

$$Wind_{sal_{cost}} = N_w \times \left[C_{wr} \times \frac{wind_{sal_f r}}{Wind_{LF}} \times \frac{1}{(1+ir)^{PRJ_{LF}}} \times \frac{ir \times (1+ir)^{PRJ_{LF}}}{(1+ir)^{PRJ_{LF}} - 1} \right] \tag{26}$$

The total WT cost is calculated as follows:

$$Wind_{cost} = N_w \times W_{OM} + Wind_{cost_c} + Wind_{cost_r} - Wind_{sal_{cost}} \tag{27}$$

The cost analysis of the wind energy component is described through Eqs. (24) to (27). In Eq. (24), the WT capital cost ($Wind_{cost_c}$) is calculated by considering the number of wind turbines (N_w) and the cost per WT unit (C_{wr}), incorporating the interest rate (ir) and project lifetime (PRJ_{LF}) to determine the amortized capital cost over the project's lifetime. Moving to Eq. (25), the WT replacement cost ($Wind_{cost_r}$) considers the lifespan of the wind turbines ($Wind_{LF}$) and the same amortization factor, calculating the replacement cost over the project's duration. The salvage value of the wind turbines at the project's end is handled in Eq. (26), where the WT salvage cost ($Wind_{sal_{cost}}$) is determined using the salvage factor ($wind_{sal_f r}$) and the remaining value of the turbines based on their useful lifespan and cost per unit. Finally, Eq. (27) calculates the annualized WT cost ($Wind_{cost}$, which sums the capital cost, replacement cost, operation and maintenance expenses ($N_w \times W_{OM}$), and subtracts the salvage value to determine the total annualized cost of the wind energy component.

The operational and maintenance expenses for the solar energy component were computed using the following methodology:

Solar Operation and Maintenance (O&M) Cost:

$$Solar_{OM_c ost} = N_{sol} \times S_{OM} \tag{28}$$

The solar capital cost is calculated as follows:

$$Solar_{C_c ost} = N_{sol} \times Cs \times \left(\frac{ir \times (1+ir)^{PRJ_{LF}}}{(1+ir)^{PRJ_{LF}} - 1} \right) \tag{29}$$

The solar annualized cost is calculated as follows:

$$Solar_{cost} = Solar_{OM_c ost} + Solar_{C_c ost} \tag{30}$$

The financial analysis of the solar energy component is described through Eqs. (28) to (30). In Eq. (28), the Solar Operation and Maintenance (O&M) Cost ($Solar_{OM_c ost}$) is calculated by multiplying the number of solar panels (N_{sol}) by the per-unit O&M cost (S_{OM}). Eq. (29) calculates the Solar Capital Cost ($Solar_{C_c ost}$) usingN_{sol}, the cost per panel (Cs), the interest rate (ir), and the project lifetime (PRJ_{LF}) to determine the amortized capital cost. Finally, in Eq. (30), the Solar Annualized Cost ($Solar_{cost}$) sums the O&M costs and capital costs to provide the total annualized cost of the solar energy component. This comprehensive approach accounts for both ongoing operational and initial investment costs.

The calculation of operational and maintenance costs associated

with the DG unit was performed in accordance with the procedure outlined below.

$$Fuel_c = 2.55 \times DG_{hr} + DG_{Pro} \times 0.251 \tag{31}$$

$$DG_{cost_c} = DG_{Size} \times \left[DG_c \times \left(\frac{ir \times (1+ir)^{PRJ_{LF}}}{(1+ir)^{PRJ_{LF}} - 1}\right)\right] \tag{32}$$

$$DG_{cost_r} = DG_{Size} \times \frac{1}{(1+ir)^{DG_{LF}}} \times \left[DG_{Rc} \times \left(\frac{ir \times (1+ir)^{PRJ_{LF}}}{(1+ir)^{PRJ_{LF}} - 1}\right)\right] \tag{33}$$

$$DG_{sal_{cost}} = DG_{Size} \times \left[DG_{Rc} \times \frac{DG_{sal_f r}}{DG_{LF}} \times \frac{1}{(1+ir)^{PRJ_{LF}}} \times \frac{ir \times (1+ir)^{PRJ_{LF}}}{(1+ir)^{PRJ_{LF}} - 1}\right] \tag{34}$$

$$DG_{cost} = DG_c + DG_{Rc} + Fuel_c - DG_{sal_{cost}} \tag{35}$$

The cost analysis for the DG component is described through Eqs. (31) to (34). In Eq. (31), the Fuel Cost ($Fuel_c$) is calculated by adding the fuel consumption rate per hour of operation (DG_{hr}) multiplied by a fuel cost factor of 2.55, and the DG production (DG_{Pro}) multiplied by 0.251. Eq. (32) computes the Capital Cost (DG_{cost_c}), which is a function of the DG size (DG_{Size}), the cost per unit (DG_c), the interest rate (ir), and the project lifetime (PRJ_{LF}), providing an amortized cost over the lifespan of the project. The replacement cost (DG_{cost_r}) in Eq. (33) is similarly based on the generator size, the replacement cost per unit (DG_{Rc}), the DG lifespan (DG_{LF}), and the interest rate, calculating the cost of replacing the generator during the project's lifetime. In Eq. (34), the salvage cost ($DG_{sal_{cost}}$) considers the remaining value of the generator at the project's end, using the replacement cost, salvage factor ($DG_{sal_f r}$), and the amortization formula, incorporating both the generator's lifespan and project lifetime. Finally, the annualized DG cost (DG_{cost}) is calculated by summing the capital cost, replacement cost, and fuel cost, and subtracting the salvage cost, providing a comprehensive assessment of the diesel generator's annualized cost over the project duration.

The inverter capital cost is calculated as follows:

$$Inverter_C = INV_{size} \times \left(INV_C \times \frac{ir \times (1+ir)^{PRJ_{LF}}}{(1+ir)^{PRJ_{LF}} - 1}\right) \tag{36}$$

The inverter replacement cost is calculated as:

$$Inverter_{Cr} = INV_{size} \times \left[INV_{Cr} \times \left(\frac{1}{(1+ir)^{INV_{LF}}}\right) \times \left(\frac{ir \times (1+ir)^{PRJ_{LF}}}{(1+ir)^{PRJ_{LF}} - 1}\right)\right] \tag{37}$$

The inverter operation and maintenance cost are respectively calculated as follows:

$$Inverter_{OM} = INV_{size} \times INV_{OM} \tag{38}$$

The inverter salvage fraction is calculated as:

$$INV_{sal_f r} = |INV_{LF} - PRJ_{LF}| \tag{39}$$

The inverter salvage cost is calculated as:

$$Inverter_{sal_C} = INV_{size} \times \left(INV_C \times \frac{INV_{sal_f r}}{INV_{LF}} \times \frac{1}{(1+ir)^{PRJ_{LF}}} \times \frac{ir \times (1+ir)^{PRJ_{LF}}}{(1+ir)^{PRJ_{LF}} - 1}\right) \tag{40}$$

The total inverter cost is calculated as follows:

$$Inverter_{Tcost} = Inverter_C + Inverter_{Cr} + Inverter_{OM} - Inverter_{sal_C} \tag{41}$$

The financial analysis for the inverter component is described through Eqs. (36) to (41). In Eq. (36), the inverter capital cost ($Inverter_C$) is calculated by multiplying the inverter size (INV_{size}) by the unit cost of the inverter (INV_C), along with the amortization factor, which includes the interest rate (ir) and the project lifetime (PRJ_{LF}). Eq. (37) calculates the inverter replacement cost (INV_{Cr}) using the inverter size, the replacement cost per unit (INV_{Cr}), and the inverter lifespan (INV_{LF}), alongside the interest rate and project lifetime. The inverter operation and maintenance cost (INV_{OM}) in Eq. (38) is straightforwardly computed by multiplying the inverter size by the per-unit operation and maintenance cost (INV_{OM}). In Eq. (39), the inverter salvage fraction ($INV_{sal_f r}$) is calculated based on the difference between the inverter lifespan and the project lifetime. This factor is used in Eq. (40), which computes the inverter salvage cost ($Inverter_{sal_C}$), accounting for the inverter size, unit cost, and amortization over the project lifetime. Finally, Eq. (41) calculates the total inverter cost ($Inverter_{Tcost}$) by summing the capital cost, replacement cost, and operational costs, while subtracting the salvage cost, providing the total cost for the inverter component over the project's lifecycle.

The grid-purchased energy cost is calculated as:

$$Grid_{cost} = \sum \left(E_{grid_p}\right) \times 0.25 - \sum \left(E_{grid_s}\right) \times 0.01 \tag{42}$$

Eq. (42), referred to as $Grid_{cost}$ defines the computational framework for evaluating the net financial cost arising from bidirectional energy exchanges between the hybrid system and the utility grid. This formulation incorporates both the COE drawn from the grid and the revenue generated from excess energy exported back to it. Specifically, $Grid_{cost}$ is computed by multiplying the total energy imported from the grid E_{grid_p}, by a unit price of 0.25, and subtracting the monetary value of the total energy exported E_{grid_s}, credited at 0.01 per unit. This pricing structure reflects a common economic asymmetry in grid-connected energy systems, wherein the cost of procuring electricity from the grid exceeds the compensation received for selling surplus energy. The equation thus effectively quantifies the financial burden imposed by grid reliance and underscores the economic advantage of minimizing grid imports while maximizing self-sufficiency in energy generation.

4. Methodology

The performance of a HRES is primarily governed by the output behavior of RESs and the demand characteristics of the associated load. These two components form the core inputs that determine the net energy balance within the system. Since RES output is intrinsically linked to location-specific meteorological conditions, the sizing of hybrid system components becomes a function of environmental variables such as solar irradiance, wind speed, and ambient temperature, as formulated in Eq. (1). Thus, proper HRES design necessitates accurate incorporation of climate-dependent inputs into system modeling.

This section outlines the methodological framework adopted in this study. It introduces the metaheuristic algorithms utilized for component sizing, explains the procedures followed in configuring the system architecture, and describes the energy management strategies employed to ensure stable operation under dynamic generation and load conditions. The mathematical formulation of the objective functions and associated constraints is provided separately in Section 3.3.

Four metaheuristic algorithms—Moth-Flame Optimization Algorithm (MFOA), WOA, Flower Pollination Algorithm (FPA), and Genetic Algorithm (GA)—were selected for performance benchmarking. These algorithms were chosen based on their algorithmic diversity and demonstrated effectiveness in engineering optimization problems, including HRES design. MFOA uses flame-based spiral search mechanisms, WOA simulates bubble-net hunting behavior of whales to balance exploration and exploitation, FPA leverages Lévy flight-based pollination dynamics, and GA applies evolutionary principles such as crossover and mutation to navigate the solution space.

The comparative use of these algorithms allows for an objective evaluation of convergence efficiency and solution quality under consistent system modeling constraints. To maintain fairness, all algorithms were implemented using fixed parameter values obtained from relevant literature, and no algorithm-specific tuning was performed. Although parameter sensitivity analysis can offer further insight into

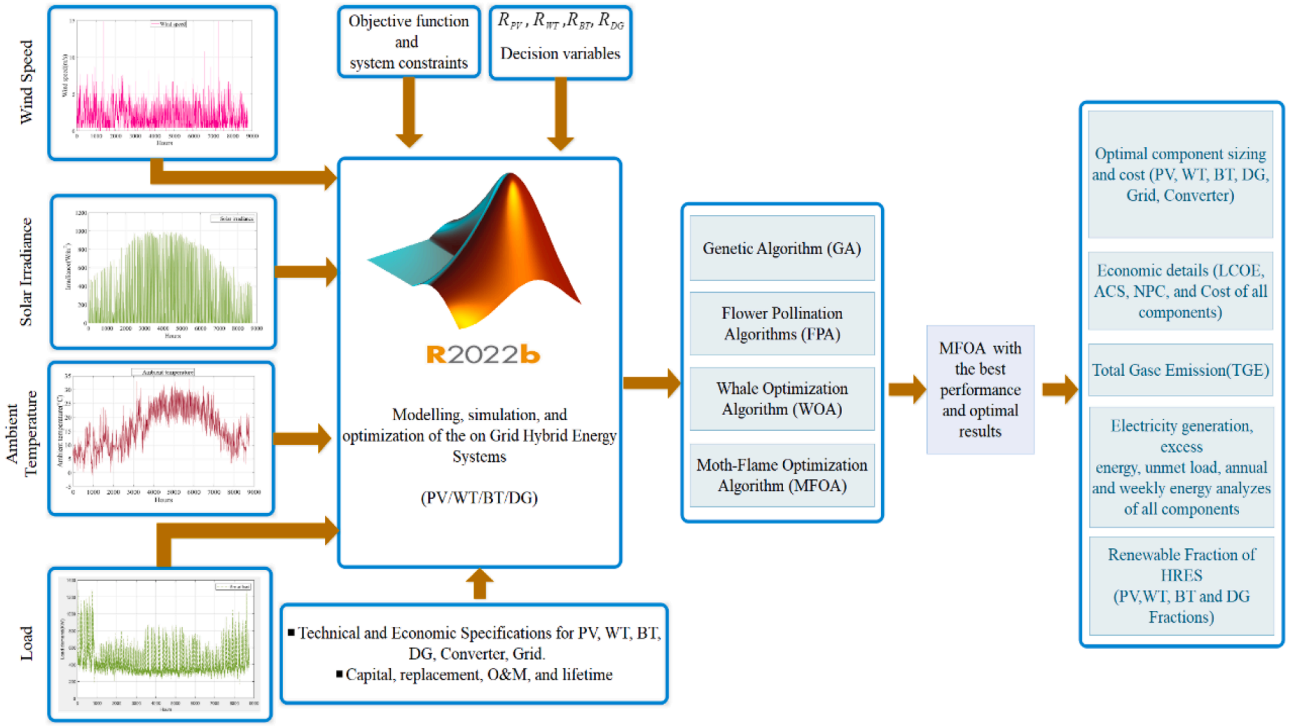

Fig. 4. Sizing Methodology.

algorithm robustness, it was deliberately excluded to avoid biasing the benchmarking process. Future studies may consider such analyses as part of adaptive algorithm design for HRES optimization.

4.1. HRES sizing and optimization

The process of Hybrid Renewable Energy System (HRES) sizing can be approached through a variety of optimization methodologies, depending on the specific parameters prioritized in a given study. Energy optimization models serve as analytical frameworks that support strategic energy planning by projecting the possible configurations and performance of energy systems under defined conditions [56]. These models not only enable the evaluation of technological feasibility but also facilitate long-term planning by incorporating structural dynamics and policy recommendations [57].

In this research, MATLAB was employed as the computational platform to streamline the optimization process and determine the most efficient system configuration for the selected geographical site. The modeling procedure required high-resolution hourly input data, including meteorological parameters (ambient temperature, solar irradiance, and wind velocity), the electrical load profile of the case study, and the techno-economic specifications of each system component [58]. The overall architecture of the input-output flow and the algorithms implemented during the sizing phase are schematically presented in Fig. 4.

4.2. Energy management system

A robust Energy Management System (EMS) is a pivotal element in microgrid design. The variable outputs exhibited by RESs, owing to their nature, underscore the importance of an effective EMS. Its main objective, with the established operational strategy in mind, is to manage the power flow among different microgrid components [59].

The operational strategy leverages various mechanisms and modes to ensure an optimal energy distribution and utilization. In this study, we designed an EMS controller based on a rule-driven algorithm tailored to a specific microgrid model. The well-defined operational modes of the EMS controller are as follows:

Mode 1: In this mode, the energy load demand is directly satisfied by the power produced by the WT and PV resources. Any excess energy is used to charge the BT if the BT energy remains below its maximum threshold. ($E_{Batt}(t) < E_{Batt\_max}(t)$)

Mode 2: When RE generation surpasses the load demand ($(Pw + Ps * uinv) \geq P_L$) and the BT reaches its full capacity ($E_{Batt}(t) = E_{Batt\_max}(t)$), the surplus energy is fed back to the grid, thus ensuring no waste of the generated RE.

Mode 3: This mode is triggered when the energy generated by the WT and PV resources does not satisfy load demand ($E_{Batt}(t) > E_{Batt\_min}(t)$). In such cases, the energy stored in the BT is used to compensate for the shortage.

Mode 4: The BT is exhausted, and the energy generated by the WT and PV resources is insufficient to meet the load demand ($E_{Batt}(t) < E_{Batt\_min}(t)$). To meet the load demand, the energy is drawn from either the DG or the grid. An optimization algorithm determines whether the DG operation or grid energy use will be used. An option that is more affordable or practical is chosen for use.

Fig. 5 presents a schematic representation of the flow algorithm for the selected HRES model. It succinctly portrays the intricate decision-making process, highlighting the interactions among various components based on the real-time energy dynamics. Fig. 6 shows the charge operational strategy. Through its flowchart, it meticulously outlines the sequence of operations that the EMS follows during periods of surplus energy. Fig. 7 pivots the discharge operational strategy, laying out the systematic approach that the system adopts when facing a deficit in the generated energy.

Collectively, these figures provide readers with a comprehensive overview of the microgrid's energy management mechanisms, emphasizing the equilibrium between generation, storage, and consumption.

4.3. Genetic algorithm (GA)

GA is a biological evolution model or construct that was created by John Holland et al. in the 1960s and the 1970s, and is founded upon

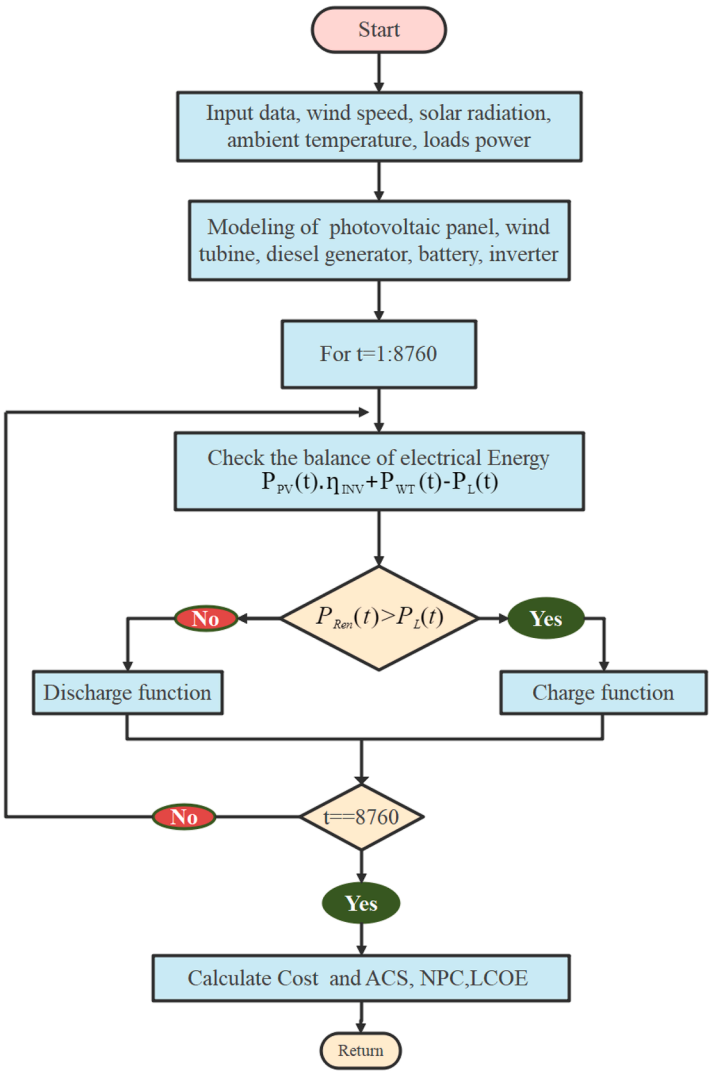

Fig. 5. Grid-connected hybrid power system design flow chart.

Charles Darwin's natural selection theory. Hollands were likely the first to study adaptive and artificial systems using the concepts of crossover, recombination, mutation, and selection. These genetic operators are fundamental building blocks of the GA. Since then, numerous variations of genetic algorithms have been created and used to solve a broad spectrum of optimization problems, from financial markets to multi-objective engineering optimization, and from graphic coloring to pattern recognition. In many optimization techniques, researchers carefully move from one point in the decision space to another while making decisions based on a set of transition rules. This point-to-point technique poses a risk because it may produce the wrong optimum in a multioptimum search space. Compared to point-to-point methods, GAs operate based on a rich database of points that climb concurrently parallel to numerous optima, which reduces the likelihood of finding a false optimum [60]. In Fig. 8, the pseudocode for the GA is presented. The steps listed below show how the GA operates [61].

1. The initial population or solution space containing potential solutions was characterized.
2. A fitness function is used to assess each solution in the population. The search was terminated if the stopping criterion was satisfied. If not, proceed to the next action.
3. The best solutions are retained for the following generation, whereas the rest are eliminated.
4. Using crossover and mutation operators, new individuals are created in the third step from the stored individuals. The population size produced in this step matches that of the starting population.
5. As mentioned in the second step, the new population was reevaluated. The algorithm is stopped if the stopping criterion is satisfied or the maximum number of iterations has been completed; otherwise, steps 3–5 are repeated.

The Genetic Algorithm (GA) employs biologically inspired operators such as crossover and mutation to evolve candidate solutions. In this study, GA was configured with a population size of 40 and run for 100 iterations, providing a stable computational baseline for performance comparison.

The crossover probability was set to $Pc = 0.8$, enabling extensive mixing of genetic material between parent solutions. The mutation probability was chosen as $Pm = 0.2$, introducing variability and helping the algorithm explore less-visited regions. The distribution indices $\eta c = 20$ and $\eta m = 20$ were used to control the spread of crossover and mutation effects, respectively. Higher values encourage small, localized adjustments to maintain solution feasibility.

All decision variables were constrained by the same lower and upper bounds used in other algorithms. These parameters reflect commonly accepted values in GA literature and were applied without tuning to ensure comparability.

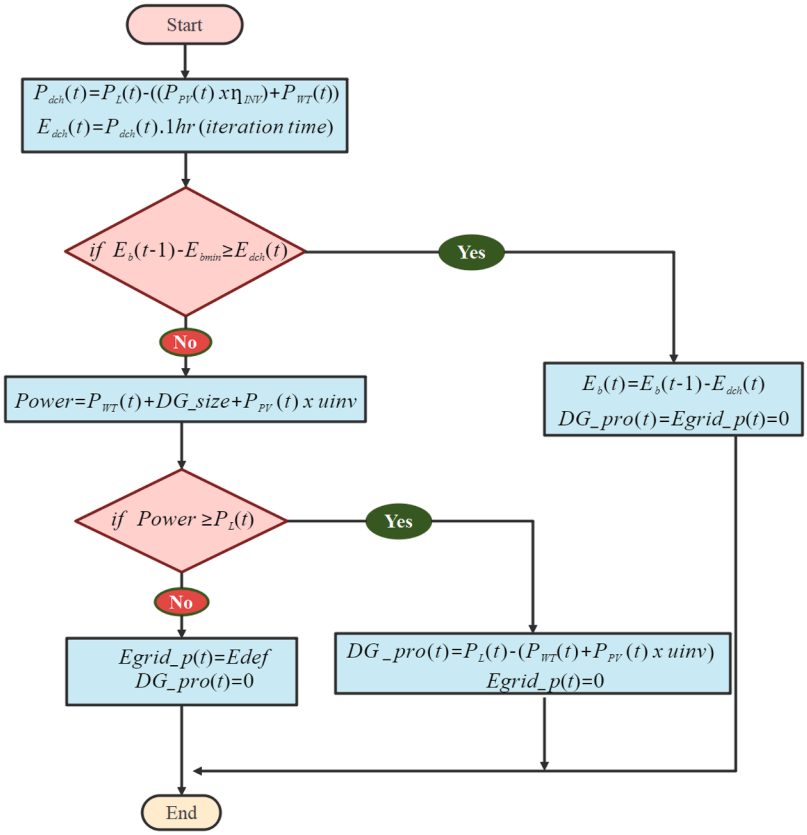

Fig. 6. Discharge function flow chart.

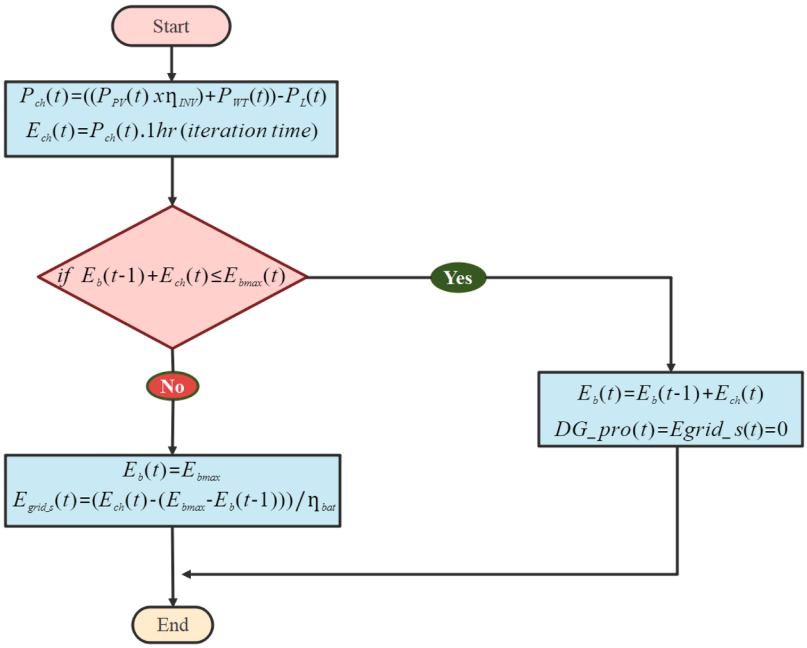

Fig. 7. Charge function flow chart.

4.4. Flower pollination algorithm (FPA)

Researchers have used various strategies because analytical methods often fail to solve complex structural problems. Heuristic and meta-heuristic optimization techniques have been used to solve various issues to produce the optimum outcome in the shortest amount of time. Based on the idea that the goal of flowers in evolution is the survival of the species and production of the most suitable population in terms of quantity and quality, the Flower Pollination Algorithm (FPA) was proposed by Yang in 2012 [62]. This algorithm is a meta-heuristic method developed based on inspiration from the reproduction process of flowering plants. The primary goal of flower pollination is to provide the best

Genetic Algorithm

1. Set parameters
2. Choose encode method
3. Generate the initial population
4. **While** i<MaxIteration and Best fitness< MaxFitness
5. **Do**
6. Fitness calculation
7. Selection
8. Crossover
9. Mutation
10. **End While**
11. Decode the individual fitness
12. **return** the optimal obtained (best)solution

Fig. 8. Pseudo-code of GA.

vitality and biological reproductive stages. There are two types of pollination, biotic and abiotic. Ten percent of all species carry out abiotic reproduction, which involves reproduction without a pollinator, whereas nearly 90 % of all species use the biotic method of pollination and reproduce by transporting pollen with the aid of organisms such as birds and insects. The remaining, very small proportion of flowering plants makes use of natural phenomena such as wind and water diffusion to reproduce.

There are two different pollination methods, cross-pollination and self-pollination. Although pollen from various flowers is used in cross-pollination, self-pollination uses either pollen produced by the plant itself or pollen from a different flower of the same species. Utilizing natural pollinators such as bees, cows, and birds, biotic pollination can occur at a distance from their origin. Although this process is global, the motion traits of a carrier resemble those of a Lévy flight. Using the four fundamental principles described below, a flower pollination algorithm was created to resolve engineering problems.

1. In accordance with the Lévy flight of the carriers, biological and cross-pollination is the global pollination process.
2. Local pollination is referred to as abiotic pollination or spontaneous pollination.
3. The flower constant varies in proportion to how closely related different flower species are, and it is expressed as the probability of reproduction.
4. A transition probability variable with a value in the range of [0–1] controls both local and global pollination processes.

Although each species produces multiple flowers and each flower contains billions of pollen gametes in the real world, the algorithm is constructed under the assumption that each species produces only one flower and one pollen gamete per flower. Thus, it is no longer necessary to express and determine pollen separately. The mathematical expression for the flower constant is given by Eq. (43).

$$x^{t+1} = x_i^t + \gamma L(\lambda)\left(g^* - x_i^t\right) \tag{43}$$

Here, x^{t+1} is the solution vector, g* is the best available solution, and γ ad is the step-size adjustment factor.

To account for pollination force, the Lévy distribution was used. Insect movement can be depicted using the Lévy distribution as insects travel long distances. Eq. (44) provides Lévy's mathematical expression.

$$L \sim \frac{\lambda\Gamma(\lambda)\sin\frac{\pi\lambda}{2}}{\pi}\frac{1}{S^{1+\lambda}},\ (s \gg s_0 > 0) \tag{44}$$

where $\Gamma(\lambda)$ is the standard gamma function (i.e., s step size). This distribution is valid for steps where $s > 0$. In theory, $s_0 \gg 0$ is necessary; however, it can be as small as s_0 0.1. Eq. (45) illustrates Rule 2 and Rule 3 for local pollination.

$$x^{t+1} = x_i^t + \in \left(x_j^t - x_k^t\right) \tag{45}$$

Here, x_i^t and x_k^t are the pollen types from different flowers of the same plant species.

The most crucial aspect of this optimization algorithm is its use of the Lévy distribution to search for numerous solution points in the search space. The optimization logic of the algorithm entails using the biotic pollination model, as used in flowers, to identify the solution points at a great distance, and using the abiotic pollination model to look into the area around the solution points. The working steps of the algorithm are illustrated in the pseudo-code provided below in Fig. 9 [63].

The FPA is inspired by the natural pollination process, where global and local pollination modes are alternated probabilistically. In this

Objective min or max f(x), x = (x1, x2…,xd)
Initialize a population of n flowers/pollen gametes with random solutions
Find the best solution g* in the initial population
Define a switch probability p ∈ [0, 1]
while(t < MaxGeneration)
for i* = 1 : *n (all n flowers in the population)
if $rand < p$
Draw a (d-dimensional) step vector L from a L´evy distribution
Global pollination via $x^{t+1} = x_i^t + \gamma L(\lambda)(g^* - x_i^t)$
else
Draw ε from a uniform distribution in [0,1])
Do local pollination via $x^{t+1} = x_i^t + \varepsilon\,(x_j^t - x_k^t)$
end if
Evaluate new solutions
If new solutions are better, update them in the population
end for
Find the current best solution $g*$
end while
Output the best solution found

Fig. 9. Pseudo-code of FPA.

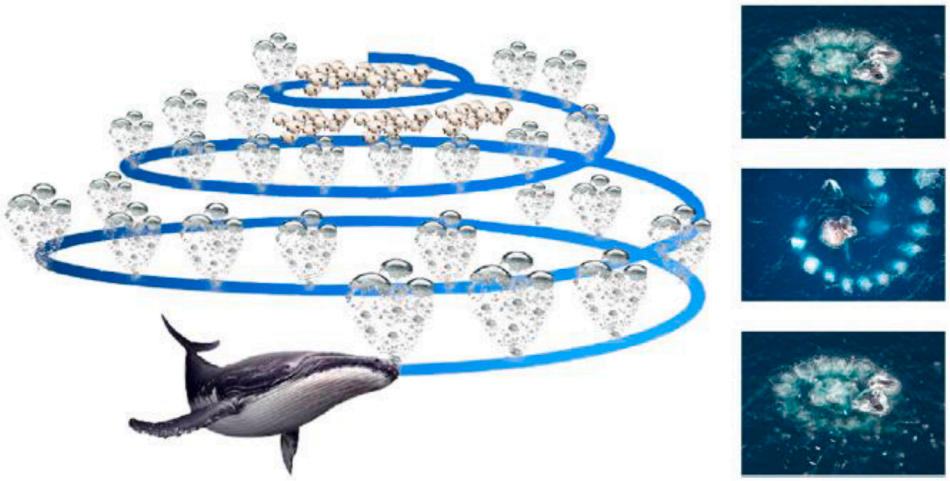

Fig. 10. Bubble net hunting technique [64].

work, the algorithm was executed with 40 population members and 100 iterations, in accordance with the general optimization framework of the study.

The switching probability $p = 0.8$ prioritizes global search using Lévy flight, simulating the long-distance movement of pollinators. The Lévy distribution is governed by $\beta = 1.5$, allowing for occasional large jumps that help the algorithm escape local optima. Local pollination steps are performed when the random threshold falls below p, encouraging fine-tuning around promising regions.

These parameter choices enhance the algorithm's capability to navigate complex search landscapes. Lower and upper bounds for decision variables were maintained identically to the other metaheuristics. No parameter tuning was applied to preserve benchmark neutrality.

4.5. Whale optimization algorithm (WOA)

The WOA, introduced by Mirjalili and Lewis in 2016, is a population-based metaheuristic inspired by the unique hunting techniques of humpback whales. Despite being a relatively recent addition to the field of optimization, WOA has found widespread application in solving complex engineering problems across diverse domains such as clustering, classification, image processing, networking, and task scheduling [59].

The algorithm emulates the specialized bubble-net hunting strategy employed by humpback whales, which predominantly feed on small fish and krill. This strategy involves the generation of bubble clouds through coordinated exhalation while the whale swims upward. These spiraling bubble structures serve to confuse and encircle prey, gradually narrowing the radius as the whale ascends toward the surface. The shrinking bubble ring not only conceals the predator's approach but also facilitates the localization, immobilization, and eventual capture of the prey [65].

This natural hunting behavior has been abstracted into the WOA's search mechanism. As visualized in Fig. 10, the spiral bubble-net technique enables whales to enclose targets near the water's surface using helical movements and concentric formations. This biologically inspired process has been mathematically translated into the core exploitation phase of the WOA, which governs local search and convergence around optimal candidate solutions.

Within the framework of the WOA, the "hunt" metaphorically represents the optimal solution to the given problem, whereas each individual whale agent corresponds to a feasible candidate solution within the search space. The optimization process initiates with a population of agents defined by the user and iteratively refines their positions based on the location of the currently best-performing agent. This process continues until the predefined number of iterations is completed, thereby enabling a systematic exploration and exploitation of the solution space.

The WOA is structurally composed of three distinct phases, each mathematically formulated to mimic specific natural behaviors: (i) **prey encirclement**, which facilitates convergence around promising solutions; (ii) the **bubble-net attack**, responsible for exploitation through shrinking and spiral movements; and (iii) **randomized prey search**, which enhances global exploration and mitigates premature convergence. Each component contributes uniquely to the overall search dynamics and is modeled through specific update equations that collectively define the behavior of the algorithm.

4.5.1. Encirclement mechanism

Once the optimal search agent—i.e., the one yielding the best fitness value—has been identified, the remaining agents adjust their positions relative to this leader to simulate the encirclement behavior observed in nature. This process models the convergence of the population toward the most promising region in the search space. The mathematical representation of this mechanism is described by Eqs. (46) and (47):

$$\vec{D}^{\rightarrow} = \left| \vec{C}^{\rightarrow} . \overrightarrow{X^{*}}^{\rightarrow}(t) - \vec{X}^{\rightarrow}(t) \right| \tag{46}$$

$$\vec{X}^{\rightarrow}(t+1) = \overrightarrow{X^{*}}^{\rightarrow}(t) - \vec{A}^{\rightarrow} . \vec{D}^{\rightarrow} \tag{47}$$

In these equations, t denotes the current iteration, $\overrightarrow{X^{*}}^{\rightarrow}(t)$ represents the position vector of the current best solution, and the operator '·' refers to the Hadamard (element-wise) product. The vectors $\vec{A}^{\rightarrow}$ and $\vec{C}^{\rightarrow}$ are control parameters defined by Eqs. (48) and (49), respectively:

$$\vec{A}^{\rightarrow} = 2\vec{a}^{\rightarrow}\vec{r}^{\rightarrow} - \vec{a}^{\rightarrow} \tag{48}$$

$$\vec{C}^{\rightarrow} = 2\vec{r}^{\rightarrow} \tag{49}$$

Here, $\vec{r}^{\rightarrow}$ represents a random vector that takes values in the range of [0,1], and $\vec{a}^{\rightarrow}$ is a vector that decreases from 2 to 0 over iterations.

Here, $\vec{r}^{\rightarrow}$ is a randomly generated vector with elements uniformly distributed in the interval [0,1], and $\vec{a}^{\rightarrow}$ is a linearly decreasing vector that transitions from 2 to 0 throughout the optimization process. This mechanism encourages exploitation by guiding agents toward the current best solution, thereby enhancing convergence efficiency without prematurely limiting the search space.

4.5.2. Bubble-Net feeding mechanism

As depicted in Fig. 10, the bubble-net hunting strategy in the WOA integrates two possible movement patterns: spiral motion and circular shrinkage around the prey. Each agent in the population is granted an equal probability (50 %) of executing either strategy at each iteration. The mathematical representation of the shrinking encirclement behavior is given in Eq. (48), while the spiral trajectory toward the prey is described by Eq. (50). These two approaches collectively constitute the exploitation phase of the algorithm, enhancing the local search capability around the identified best solution. The update rule for the position of the search agent is governed by a probabilistic decision process. The following equation defines the position update mechanism:

$$\vec{X}^{\rightarrow}(t+1) = \left\{ \begin{array}{l} \overrightarrow{X^{*\rightarrow}}(t) - \vec{A}^{\rightarrow}.\vec{D}^{\rightarrow}, \ if\ p < 0.5 \\ \overrightarrow{D'^{\rightarrow}}.e^{bl}.\cos(2\pi l) + \overrightarrow{X^{*\rightarrow}}(t), \ if\ p \geq 0.5 \end{array} \right\} \quad (50)$$

In this formulation, $\overrightarrow{X^{*\rightarrow}}(t)$ represents the current best solution, $\vec{A}^{\rightarrow}$ and $\vec{D}^{\rightarrow}$ are coefficient and distance vectors respectively, b is a constant defining the shape of the logarithmic spiral, and $l \in [-1,1]$ is a randomly generated number. The variable p, sampled uniformly from the interval [0,1], determines the selection between the spiral and shrinking motions. This probabilistic switching mechanism enables the algorithm to maintain a balance between intensification and diversification during the optimization process.

4.5.3. Randomized prey search strategy

Beyond employing the bubble-net feeding strategy, humpback whales are also capable of engaging in prey search through stochastic movement patterns. To simulate such behavior in the WOA, position updates are performed using a randomly selected search agent rather than the global best agent identified thus far. This mechanism utilizes vector $\vec{A}^{\rightarrow}$, where values exceeding 1 or below −1 are applied to facilitate movement away from the reference whale, thereby enhancing solution diversity.

In contrast to the spiral-shaped bubble-net mechanism, this randomized strategy aims to intensify global exploration by dynamically altering the agent's position using alternate candidates. The incorporation of $\vec{A}^{\rightarrow}$ and a randomly chosen position vector allows the algorithm to escape potential entrapment in local optima and encourages broader search space traversal. The mathematical formulation guiding this behavior is expressed by Eqs. (51) and (52):

$$\vec{D}^{\rightarrow} = \left| \vec{C}^{\rightarrow}.\vec{X}^{\rightarrow}_{rand} - \vec{X}^{\rightarrow} \right| \quad (51)$$

$$\vec{X}^{\rightarrow}(t+1) = \vec{X}^{\rightarrow}_{rand} - \vec{A}^{\rightarrow}.\vec{D}^{\rightarrow} \quad (52)$$

At each iteration, the search agent updates its location based on the randomly selected peer, treating it as the provisional best. The control parameter aaa, which regulates exploration and exploitation, linearly decreases from 2 to 0 over the course of iterations. Meanwhile, the probability parameter p-value in Eq. (50) determines whether the agent follows a circular or spiral trajectory. The algorithm concludes upon reaching the optimal solution and fulfilling the convergence condition. A detailed representation of this process is presented in the corresponding pseudocode given in Fig. 11.

The WOA mimics the bubble-net hunting strategy of humpback whales. Its performance hinges on adaptive parameters that control both exploration and exploitation. In this study, WOA was implemented using a 40-agent population over 100 iterations, aligned with the other tested algorithms for benchmarking consistency.

The coefficient a linearly decreases from 2 to 0, which regulates the balance between exploitation (shrinking encircling behavior) and exploration (random search). The parameter a2, ranging from −1 to −2, governs the logarithmic spiral movement, enhancing the algorithm's local search capability. The switching probability p determines whether the next position will be updated using direct encircling or spiral updating. A fixed $b = 1$ was used to shape the spiral pattern.

These parameters allow WOA to converge rapidly when good solutions are identified, while still enabling global search in early iterations. The solution space bounds remained consistent with the other algorithms, ensuring methodological fairness.

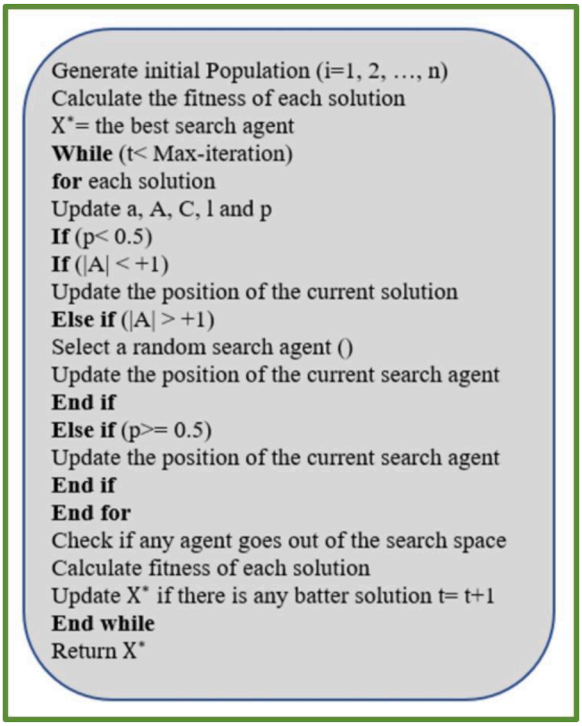

Fig. 11. Pseudo-code of the native WOA algorithm.

4.6. Moth-flame optimization algorithm (MFOA)

A metaheuristic algorithm created by Mirjalili and motivated by population theories is called the MFO algorithm. It is based on the capacity of moths to maintain a specific angle to the moon while flying straight and at night. Moths are assumed to move towards the flame in this method at a fixed angle, and they are entangled in this spiral path that leads to the flame. Moths were initially generated randomly within a set of algorithmic parameters. The best positions were then marked with frames after the fitness value was calculated. The number of flames and positions of the moths were updated after determining the distance to the corresponding moth. Once the termination criteria are satisfied, new positions are created, and the previous procedure is repeated. The

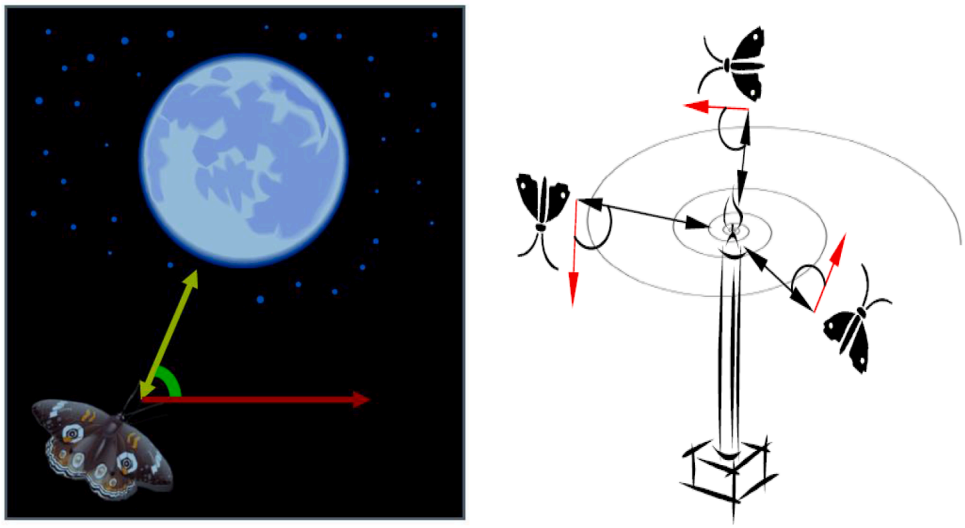

(a) (b)

Fig. 12. a) Transverse orientation, b) Flight path in a spiral that avoids nearby light sources.

position of the moth in relation to the flame at a particular moment is taken as the solution, even though the flame is considered the best option in the MFOA. All options for which there is a best optimal solution are represented by the moth population.

When a moth flies in a spiral, it is either useless or fatal because the light is close to the Moon while still maintaining a similar angle to the light source [67]. Fig. 12 presents a conceptual representation of this behavior. The moth finally approached the flame, as shown in Fig. 12. To propose an optimizer algorithm called the MFOA, this behavior is mathematically modeled in the following subsection.

4.6.1. Creation of the first moth population

The variables of the problem are the positions of the moths in space, and it is assumed that the candidate solutions in the proposed MFOA are the moths. Moths can therefore fly by modifying their position vectors in 1-dimensional, 2-dimensional, 3-dimensional, or hyper-dimensional spaces. The long moth-flame algorithm uses two populations. Therefore, six matrices were generated: two matrices for the moths (OM), two matrices for the flames (OF), and another two for the initial populations of moths (M) and flames (F) for convenience.

As a population-based algorithm, the MFOA represents the quantity of cluster moths in a matrix as follows:

$$M = \begin{bmatrix} m_{1,1} & \cdots & m_{1,d} \\ \vdots & \vdots & \vdots \\ m_{n,1} & \cdots & m_{n,d} \end{bmatrix} \tag{53}$$

Here, n represents the number of moths searched, and m represents the number of dimensions. It should be noted that both the moths and flames are solutions. This distinction lies in the manner in which we handle and update them throughout each iteration. Eq. (54) is used to record all moth fitness values.

$$OM = \begin{bmatrix} OM_1 \\ OM_2 \\ \vdots \\ OM_2 \end{bmatrix} \tag{54}$$

The remaining elements of the MFOA were the flames. Flames are depicted in the following matrix with their fitness function vectors in a 3-dimensional space:

$$F = \begin{bmatrix} F_{1,1} & \cdots & F_{1,d} \\ \vdots & \vdots & \vdots \\ F_{n,1} & \cdots & F_{n,d} \end{bmatrix} \tag{55}$$

$$OF = \begin{bmatrix} OF_1 \\ OF_2 \\ \vdots \\ OF_2 \end{bmatrix} \tag{56}$$

4.6.2. Updating moth positions

MFOA combines global optimal of optimization problems using three different functions. Eq. (57) defines these functions:

$$MFO = (I, P, T) \tag{57}$$

The function I is in charge of producing the moth matrix population and fitness values, it has no input and produces the values M and OM. This function's methodological model is represented by Eq. (58):

$$I : \varnothing \rightarrow \{ M, \quad OM \} \tag{58}$$

The main mathematical operation of this method, which moves moths through the search space, is represented by the P function. This function starts with the matrix M and returns the updated matrix.

The movement of the moth "around" the flames is the primary mathematical function represented by the function P in this approach. Updates to the input M and the output M are as follows:

$$P : M \rightarrow M \tag{59}$$

The termination criterion's role in analysis: If the termination criterion is met, T returns true; otherwise, it returns false.

$$T : M \rightarrow \{ True, \quad False \} \tag{60}$$

The algorithm begins by producing the initial solution of I using Eq. (58). Following this, Eq. (59) is used by the function P to begin updating the positions of the moths. It continues, accounting for the flames during each iteration, until T is reached.

The following formula represents the function used to perform random distribution:

$$M(i,j) = ((ub(i) - lb(i)).rand(i) + lb(i) \tag{61}$$

In light of these considerations, the MFOA's definition of a

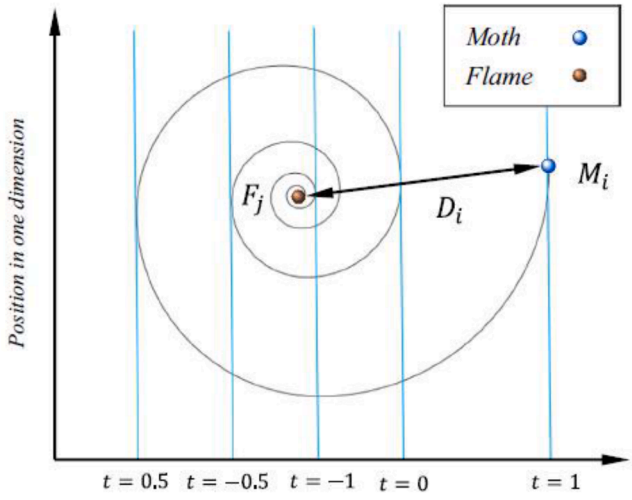

Fig. 13. Space around the flame, the logarithmic spiral, and position in relation to t [66].

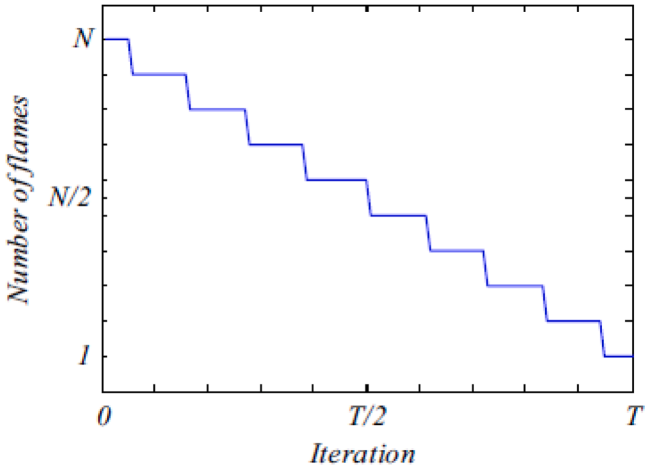

Fig. 14. Adaptive decrease in flame count over multiple iterations.

logarithmic spiral is as follows:

$$S(M_i, F_j) = D_i.e^{bt}.\cos(2\pi t) + F_j \tag{62}$$

$$D_i = |F_j - M_i| \tag{63}$$

Here, M_i is a constant that defines the ith moth, Fj is the jth flame, D_i is the distance between the jth flame and the ith moth, b is a constant value that describes the shape of the logarithmic spiral, and t is a random value in the interval of [1,1]. The 'spiraling movement of the moths in the search space of the MFOA toward the flame strikes a balance between exploitation and exploration.

Hence, the moth's curvilinear trajectory was captured using Eq. (62). This mathematical representation elucidates the subsequent positioning of each moth in relation to the flame. The parameter 't' in the spiral equation defines the proximity of the moth to the flame for upcoming positions (with t=−1 signifying the nearest and t = 1 being the most distant). This implies that a hyperelliptical zone can be envisioned around the flame, determining the moth's ensuing location within this region. The pivotal component of the introduced approach is the helical trajectory as it dictates the positional updates of moths concerning the flames. Rather than restricting a moth's movement to the space between flames, the spiral equation allows it to navigate in the vicinity of a flame. This ensures comprehensive probing and efficient utilization of the search domain. Fig. 13 presents a visualization that encapsulates the logarithmic spiral, the flame's encompassing zone, and the influence of varied 't' values on the trajectory

Generate initial Population.
Initialize Moths and evaluated their cost.
repeat
Update Flame Number
If (iteration number= 1) then
Sort the initial population of moths according to cost.
Flame Sorted moths
Else if
Merge both previous population and flames according to cost
Update flames position and their cost
End if
Else if
Update the position of best flame so far and its cost.
Previous population moths
For (all moths in current population) do
Calculate the distance to the corresponding flame.
Update moths' position with respect to its corresponding flame
End for
Until Stopping condition are met

Fig. 15. MFOA pseudo-code.

4.6.3. Updating the number of flames

This section describes how the MFOA has been improved (i.e., updating the positions of the moths at n different positions in the search space can reduce the chances of using the best optimal solutions). This issue, as expressed in Eq. (64), can be resolved by incorporating flame number reduction as an adaptive mechanism in the iteration function. This process is illustrated in Fig. 14.

$$Flame\ no = round\left(N - l * \frac{N-l}{T}\right) \tag{64}$$

where, N represents the maximum number of flames, l is the valid number of iterations, and T is the maximum number of iterations.

The MFOA relies on the navigation behavior of moths in nature, modeled mathematically as a logarithmic spiral movement around flames (candidate solutions). In the current study, MFOA was executed with a population size of 40 and 100 iterations, ensuring a consistent search effort across all tested algorithms.

The parameter a, linearly decreasing from −1 to −2 during the iterations, controls the convergence behavior by shrinking the search space. The coefficient b was set to 1, influencing the spiral shape of the moths' trajectory. The variable t introduces randomness within the logarithmic spiral, further promoting exploration. These parameter settings ensure a balanced transition from exploration to exploitation, essential for avoiding local minima.

The lower and upper bounds were set to [1, 1, 1, 1] and [5000, 5000, 800, 1000], respectively, for the four optimization variables (PV, WT, BT, DG). These bounds reflect realistic sizing ranges under techno-economic constraints. The algorithm maintained consistent performance without parameter tuning, ensuring a fair comparison with other techniques. Pseudo-code of MFOA is shown in Fig. 15.

5. Simulation results and discussion

The results of this study revealed an objective function depending on reducing the ACS, TNPC, and LCOE values of the grid-connected WT, PV, DG, and BT components of the proposed HRES. GA, FPA, WOA, and MFOA methods were used for the solution, and their performances were assessed. To meet the electricity load demand with high reliability, numerous constraints including $LPSP_{max}$, RE REF, SOC, and optimal

Table 3
Comparative Optimal Sizing using MFOA, WOA, FPA, and GA Techniques (Under $LPSP_{max}$=0.5 % Limitation).

	MFOA	WOA	FPA	GA
	$LPSP_{max}$ = 0.5%			
Execution time (*sec*)	336.5487	491.2846	555.4989	612.0884
Wind Turbines (kW)	1.000011	1	1	1
Solar Power (kW)	2.1343×10^3	2.1299×10^3	2.1317×10^3	2.1232×10^3
Battery Units	1.8998×10^2	1.9272×10^2	2.0745×10^2	2.1958×10^2
Total Wind Energy (kWh)	125.5758	125.5744	125.5744	125.5744
Total Solar Energy (kWh)	3.0918×10^6	3.0854×10^6	3.0880×10^6	3.0757×10^6
Diesel Generator Energy Generation (kWh)	–	–	–	–
Wasted Energy (kWh)	–	–	–	–
Total Load Demand (kWh)	2.1776×10^6	2.1776×10^6	2.1776×10^6	2.1776×10^6
TGE	–	–	–	–
Bat_{in} (kWh)	1.0506×10^5	1.0527×10^5	1.0412×10^5	1.0401×10^5
Bat_{out} (kWh)	1.0882×10^6	1.0877×10^6	1.0915×10^6	1.0923×10^6
LCOE ($/kWh)	0.1443	0.1443	0.1444	0.1443
Grid Sale (kWh)	1.3284×10^6	1.3222×10^6	1.3207×10^6	1.3069×10^6
Grid Purchase (kWh)	4.7337×10^5	4.7398×10^5	4.6929×10^5	4.6831×10^5
TNPC ($)	3.5085×10^6	3.5054×10^6	3.5256×10^6	3.5255×10^6
REF (%)	100	100	100	100
Annual Cost ($)	3.1426×10^5	3.1427×10^5	3.1443×10^5	3.1433×10^5
Wind Cost ($)	404.8870	404.8825	404.8825	404.8825
Solar Cost ($)	1.9214×10^5	1.9174×10^5	1.9190×10^5	1.9114×10^5
DG Cost ($)	–	–	–	–
Battery Cost ($)	1.3575×10^4	1.3771×10^4	1.4823×10^4	1.5690×10^4
Inverter Cost ($)	3.0598×10^3	3.0598×10^3	3.0598×10^3	3.0598×10^3

Table 4
Comparative Optimal Sizing using MFOA, WOA, FPA, and GA Techniques (Under $LPSP_{max}$=2 % Limitation).

	MFOA	WOA	FPA	GA
	$\boldsymbol{LPSP_{max}}$ = 2%			
Execution time (*sec*)	410.285	454.9739	429.1147	499.0886
Wind Turbines (kW)	1	1.0035	1	1
Solar Power (kW)	2.1098×10^3	2.1073×10^3	2.0751×10^3	2.1147×10^3
Battery Units	1.9076×10^2	1.9200×10^2	1.8277×10^2	1.9532×10^2
Total Wind Energy (kWh)	125.5744	126.0249	125.5744	125.5744
Total Solar Energy (kWh)	3.0562×10^6	3.0526×10^6	3.0059×10^6	3.0633×10^6
Diesel Generator Energy(kWh)	–	–	–	–
Wasted Energy (kWh)	–	–	–	–
Total Load Demand (kWh)	2.1776×10^6	2.1776×10^6	2.1776×10^6	2.1776×10^6
TGE	–	–	–	–
Bat_{in} (kWh)	1.0373×10^5	1.0388×10^5	1.0757×10^5	1.0303×10^5
Bat_{out} (kWh)	1.0724×10^6	1.0720×10^6	1.0608×10^6	1.0745×10^6
LCOE ($/kWh)	0.1427	0.1427	0.1428	0.1427
Grid Sale (kWh)	1.3085×10^6	1.3051×10^6	1.2685×10^6	1.3136×10^6
Grid Purchase (kWh)	4.6728×10^5	4.6771×10^5	4.8100×10^5	4.6466×10^5
TNPC ($)	3.4721×10^6	3.4700×10^6	3.4155×10^6	3.4839×10^6
REF (%)	100	100	100	100
Annual Cost ($)	3.1078×10^5	3.1079×10^5	3.1092×10^5	3.1085×10^5
Wind Cost ($)	404.8825	406.3348	404.8825	404.8825
Solar Cost ($)	1.8993×10^5	1.8970×10^5	1.8680×10^5	1.9037×10^5
DG Cost ($)	–	–	–	–
Battery Cost ($)	1.3631×10^4	1.3719×10^4	1.3060×10^4	1.3957×10^4
Inverter Cost ($)	3.0598×10^3	3.0598×10^3	3.0598×10^3	3.0598×10^3

Table 5
Comparative Optimal Sizing using MFOA, WOA, FPA, and GA Techniques (Under $LPSP_{max}$=5 % Limitation).

	MFOA	WOA	FPA	GA
	$\boldsymbol{LPSP_{max}}$ = 5%			
Execution time (*sec*)	422.386	477.7378	457.2875	540.7758
Wind Turbines (kW)	1	1	1.0040	1
Solar Power (kW)	2.0624×10^3	2.0589×10^3	2.0745×10^3	2.0630×10^3
Battery Units	1.8370×10^2	1.8654×10^2	2.0705×10^2	2.0471×10^2
Total Wind Energy (kWh)	125.5744	125.5744	126.0822	125.5744
Total Solar Energy (kWh)	2.9875×10^6	2.9825×10^6	3.0051×10^6	2.9885×10^6
Diesel Generator Energy (kWh)	–	–	–	–
Wasted Energy (kWh)	–	–	–	–
Total Load Demand (kWh)	2.1776×10^6	2.1776×10^6	2.1776×10^6	2.1776×10^6
TGE	–	–	–	–
Bat_{in} (kWh)	1.0154×10^5	1.0166×10^5	9.8944×10^5	1.0002×10^5
Bat_{out} (kWh)	1.0389×10^6	1.0387×10^6	1.0471×10^6	1.0441×10^6
LCOE ($/kWh)	0.1395	0.1395	0.1396	0.1395
Grid Sale (kWh)	1.2735×10^6	1.2685×10^6	1.2829×10^6	1.2687×10^6
Grid Purchase (kWh)	4.5710x $\times 10^5$	4.5739×10^5	4.4709×10^5	4.5083×10^5
TNPC ($)	3.3920×10^6	3.3903×10^6	3.4344×10^6	3.4158×10^6
REF (%)	100	100	100	100
Annual Cost ($)	3.0382×10^5	3.0383×10^5	3.0398×10^5	3.0386×10^5
Wind Cost ($)	404.8825	404.8825	406.5198	404.8825
Solar Cost ($)	1.8566×10^5	1.8535×10^5	1.8675×10^5	1.8572×10^5
DG Cost ($)	–	–	–	–
Battery Cost ($)	1.3126×10^4	1.3329×10^4	1.4795×10^4	1.4628×10^4
Inverter Cost ($)	3.0598×10^3	3.0598×10^3	3.0598×10^3	3.0598×10^3

Table 6
Comparative Optimal Sizing using MFOA, WOA, FPA, and GA Techniques (Under $LPSP_{max}$=10 % Limitation).

	MFOA	WOA	FPA	GA
	$LPSP_{max}$ = %10			
Execution time (*sec*)	403.852	451.6854	484.0282	521.4372
Wind Turbines (kW)	1	1.0722	1	1
Solar Power (kW)	1.9802×10^3	1.9805×10^3	1.9682×10^3	1.9870×10^3
Battery Units	1.7200×10^2	2.0185×10^2	1.9872×10^2	1.8823×10^2
Total Wind Energy (kWh)	125.5744	134.6532	125.5744	125.5744
Total Solar Energy (kWh)	2.8685×10^6	2.8689×10^6	2.8512×10^6	2.8784×10^6
Diesel Generator Energy(kWh)	–	–	–	–
Wasted Energy (kWh)	–	–	–	–
Total Load Demand (kWh)	2.1776×10^6	2.1776×10^6	2.1776×10^6	2.1776×10^6
TGE	–	–	–	–
Bat_{in} (kWh)	9.8100×10^4	9.5981×10^4	9.7374×10^4	9.6341×10^4
Bat_{out} (kWh)	9.8255×10^5	9.8977×10^5	9.8557×10^5	9.8824×10^5
LCOE ($/kWh)	0.1342	0.1342	0.1342	0.1342
Grid Sale (kWh)	1.2114×10^6	1.2038×10^6	1.1899×10^6	1.2154×10^6
Grid Purchase (kWh)	4.4086×10^5	4.3208×10^5	4.3709×10^5	4.3398×10^5
TNPC ($)	3.2542×10^6	3.2876×10^6	3.2670×10^6	3.2813×10^6
REF (%)	100	100	100	100
Annual Cost ($)	2.9214×10^5	2.9222×10^5	2.9226×10^5	2.9216×10^5
Wind Cost ($)	404.8825	434.1547	404.8825	404.8825
Solar Cost ($)	1.7826×10^5	1.7829×10^5	1.7719×10^5	$1.7888\ 10^5$
DG Cost ($)	–	–	–	–
Battery Cost ($)	1.2291×10^4	1.4423×10^4	1.4199×10^4	1.3450×10^4
Inverter Cost ($)	3.0598×10^3	3.0598×10^3	3.0598×10^3	3.0598×10^3

system sizing were taken into account during the optimization process of the HRES with the PV/WT/DG/BT components. A sensitivity analysis was performed in the simulation to ascertain the impact of various $LPSP_{max}$ values on system performance. The values of ACS, TNPC, and LCOE decreased when the configurations of the LPSP values of 0.5 %, 2 %, 5 %, and 10 % were examined. The outputs of the optimization process are presented in Tables 3, 4, 5, and 6.

The energy cost findings obtained in this study demonstrated consistency with those reported in previous literature. For instance, Güven et al. [8] examined an off-grid hybrid system comprising PV, WT, (DG, and BT components for geographical regions comparable to the one analyzed here in Their study, which assumed a LPSP of zero, utilized the harmony search optimization algorithm and yielded the following results: a LCOE of $0.2012/kWh, TNPC of $6.5027 $\times$ 10^6, ACS of $4.0084 $\times$ 10^5, and wasted energy totaling 1.8431 $\times$ 10^6 kWh. Additionally, Güven and Samy [9] performed a separate techno-economic assessment involving off-grid fuel cell (FC), biomass gasifier (BG), WT, and PV units. Through application of the hybrid firefly genetic algorithm (HFGA), the optimal system configuration was found to include 1094.68 kW of wind capacity, 2256.17 kW of PV capacity, and 775 hydrogen storage units, resulting in an ACS of $2921,702.30, a TNPC of $2.4639 $\times$ 10^7, and an LCOE of $1.3416/kWh. Compared to these previous works, the proposed system developed using the Modified Firefly Optimization Algorithm (MFOA) in the present study exhibited superior performance in terms of cost efficiency, optimal sizing of RESs, and convergence speed. As presented in Table 3, the LCOE for the proposed HRES configuration was calculated to be $0.1443/kWh, with a TNPC of $3.5085 $\times$ 10^6 and an ACS of $3.1426 $\times$ 10^5. The REF achieved a full 100 %, while the maximum allowable $LPSP_{max}$ was constrained to 0.5 %. Furthermore, a total of 1.3284 $\times$ 10^6 kWh of surplus energy was exported to the utility grid, contributing to continuous annual revenue generation.

The total cost, maintenance and operating costs, project lifespan, quantities and costs of every hybrid power system generation component before the project is started, and similar factors are all price details. The designs of the MFOA, WOA, FPA, and GA methods, which are shown in Table 3, were developed separately, and the results were evaluated to achieve solutions with high accuracy in the shortest amount of time.

Considering the findings of the optimization, the proposed system utilizes solar and wind energy resources, batteries, and a grid to meet the total energy demand. This led to the conclusion that it is the most economically, technically, environmentally, and socially viable hybrid system. The annual average monthly energy balance is shown in Fig. 16. The use of solar and wind energy seems to be consistent with available resources. As seen here, the load was met by PV, BT, and the grid for 7 of the 12 months of the year (January, February, March, April, October, November, and December) and without purchasing from the grid for the remaining 5 months.

Three other metaheuristic algorithms, GA, FPA, and WOA, were

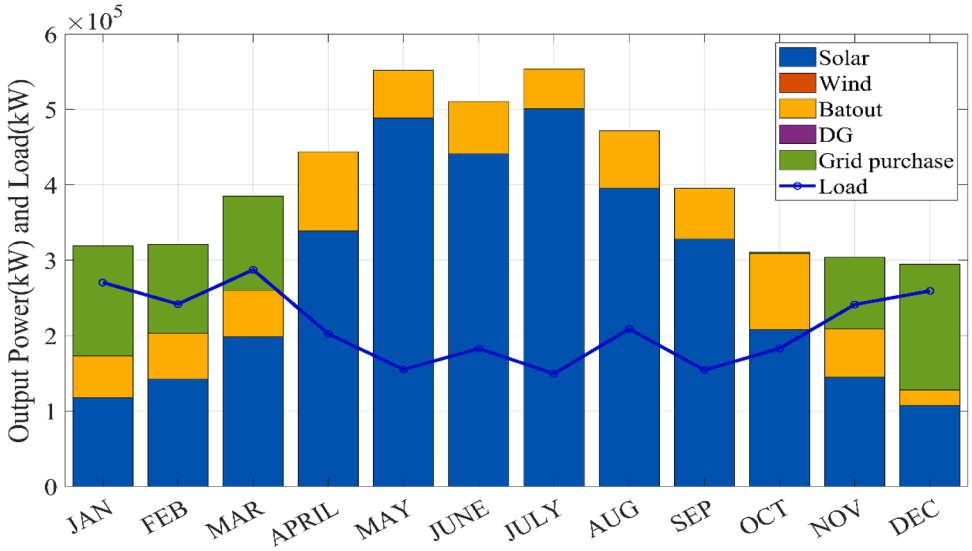

Fig. 16. Average electrical load served for optimal configuration and share of HRES components.

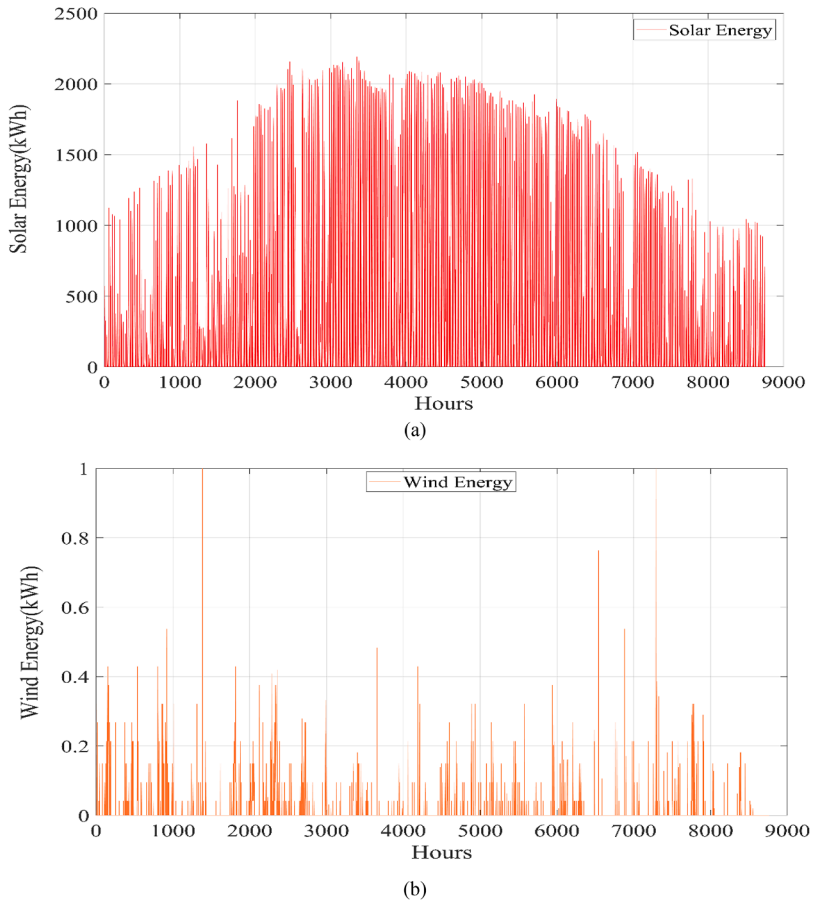

Fig. 17. (a) Average hourly solar energy, (b) Average hourly wind energy.

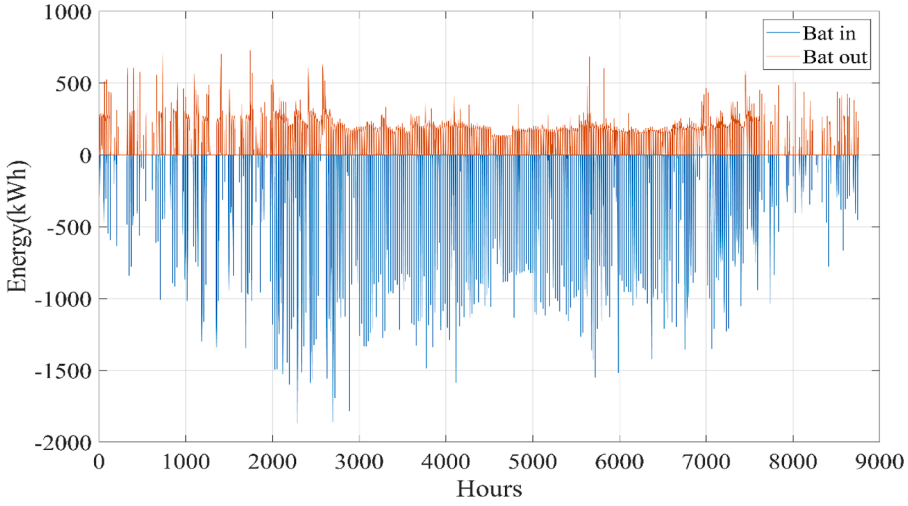

Fig. 18. Input and output energy fluctuations of BT on an hourly basis.

programmed and employed for the microgrid system design problem to ensure the validity and reliability of the proposed MFOA in determining the best sizing results of the grid-connected HRES. The results obtained were compared with those from the proposed MFOA, and the convergence characteristics of the algorithms were assessed. The values of ACS, LCOE, and TNPC decreased over the course of the iterations. This indicates that the optimization algorithm reduces the components of the objective function by heading in the direction of the optimum system size. Any reduction in the objective function was, therefore, significant, mainly because it became possible to know more about the optimum size. A thorough analysis of the convergence processes of the algorithms for the hybrid microgrid system's optimum design revealed that the MFOA performed the optimization process quickly, reducing computation time and resource consumption while producing a better outcome. As shown by the outcome presented in Table 3, MFOA offered the least expensive solution in comparison to the other algorithms while producing outcomes that were superior to those of the other algorithms. Using the MFOA, 2.109805 $\times$ 10^3 kW solar panels, a 1 kW WT, and

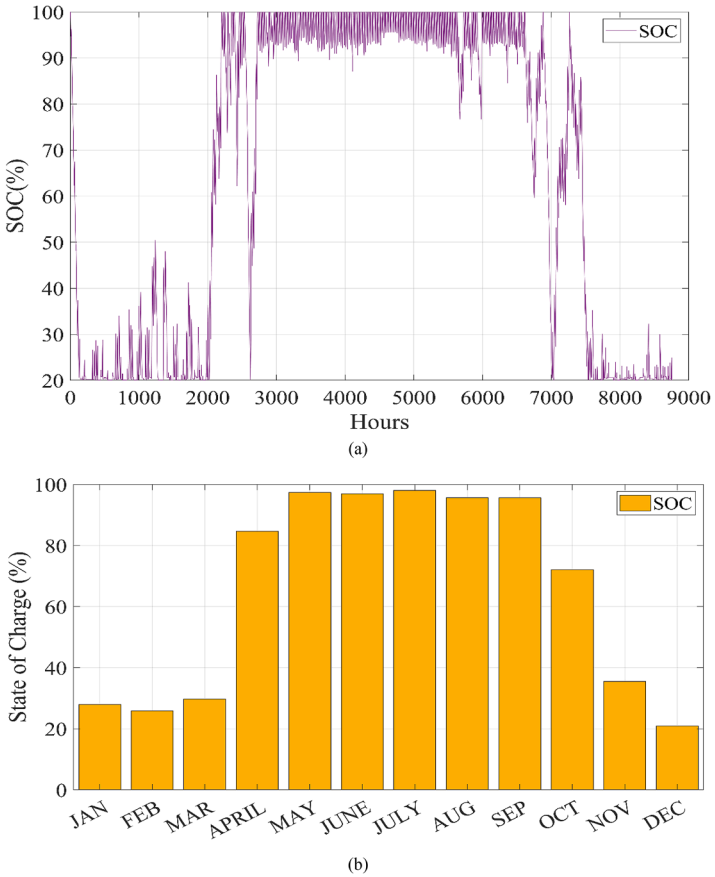

Fig. 19. a) Hourly variation of SOC, b) Average monthly variation of SOC.

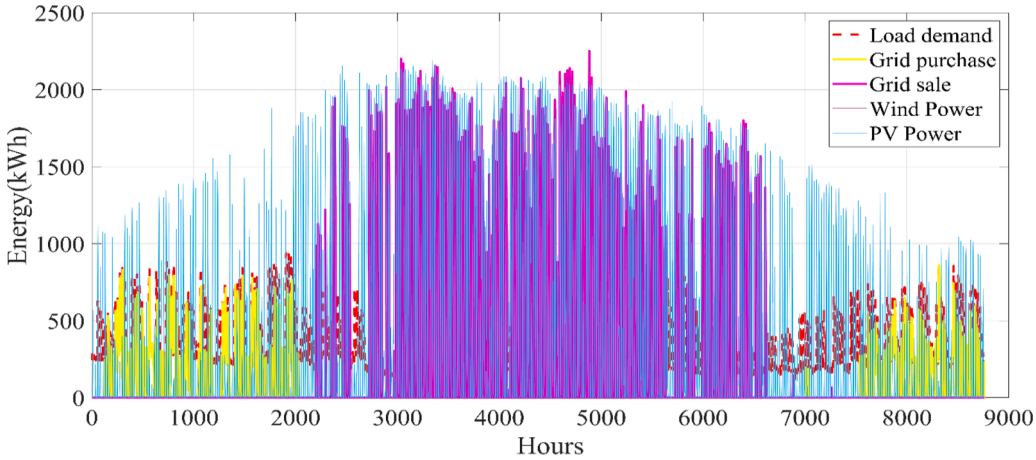

Fig. 20. A year-long comparison of energy resources and electrical load demand.

1.907645×10^2 batteries based on a 0.5 % LPSP were found to be the optimum HRES optimization results. In this process, ACS was found to be $\$3.1078 \times 10^5$, TNPC was $\$3.4721 \times 10^6$, and LCOE was \$0.1427. It should be stated that the HRES had solar panel- and BT-weighted components because the analyses were based on KW. Additionally, energy was purchased from a 4.6728×10^5 kWh grid throughout the year. Furthermore, 1.3085×10^6 kWh of energy sales was completed. This is evident in this optimization variable, as it was established within the lower (1 kW) and upper (5000 kW) limit values of the WT component. It was concluded that MFOA and other optimization-based algorithms can be successfully utilized to identify the best solution to the challenging issue of microgrid design.

The plots of PV output energy in Fig. 17(a), WT output energy in Fig. 17(b), and battery input-output energy in Fig. 18 are provided for the optimal system configuration that was determined. The system can be monitored for 8760 h from these plots, and the data points at each time value t can be observed.

The SOC is a pivotal parameter for HRES. This significance arises from the fact that the operational capacity and efficiency of the BT components, which are utilized for energy storage in HRES, are directly related to this value. SOC represents the current energy capacity of a BT in percentage terms, offering crucial insights into how much energy an HRES can generate or store. Fig. 19(a) depicts the details of the weekly and annual SOC values for BT, while also visually representing the time

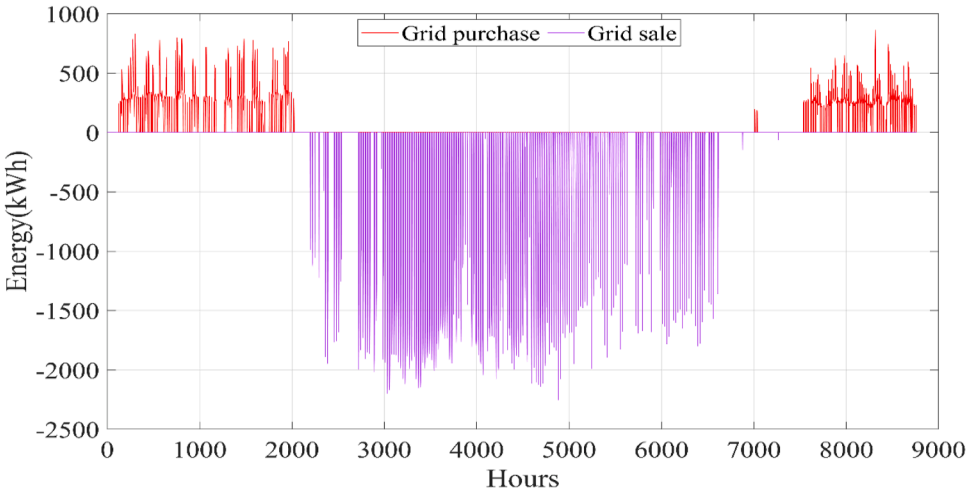

Fig. 21. Comparison of the energy that HRES sold to the grid and that it received from the grid.

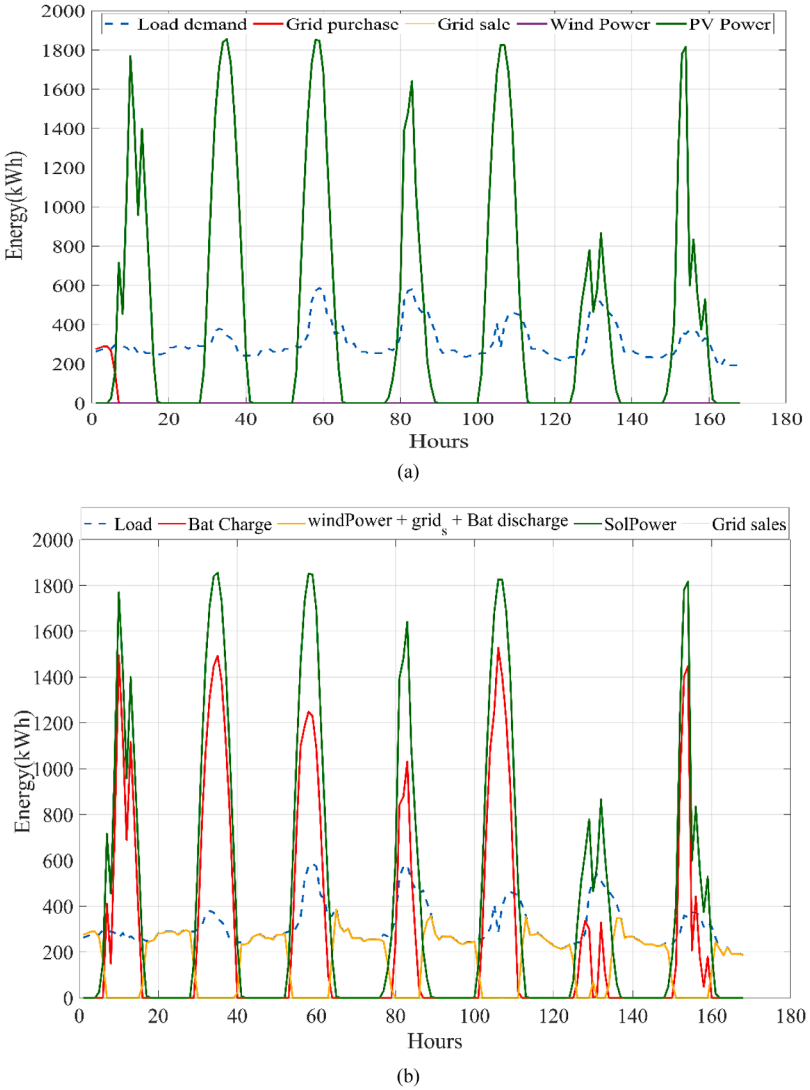

Fig. 22. HRES weekly energy analysis a) load demand, grid purchase, grid sales, WT, PV power, b) load demand, BT charge, PV power, grid sales, WT, BT discharge.

intervals in which BT achieved its minimum (SOC_{min}) and maximum (SOC_{max}) values throughout the year. These figures are essential in determining the periods where the system operated optimally based on energy needs and storage capacity or when there was an increased demand for energy.

The annual profile of the average SOC of the BT is shown in Fig. 19

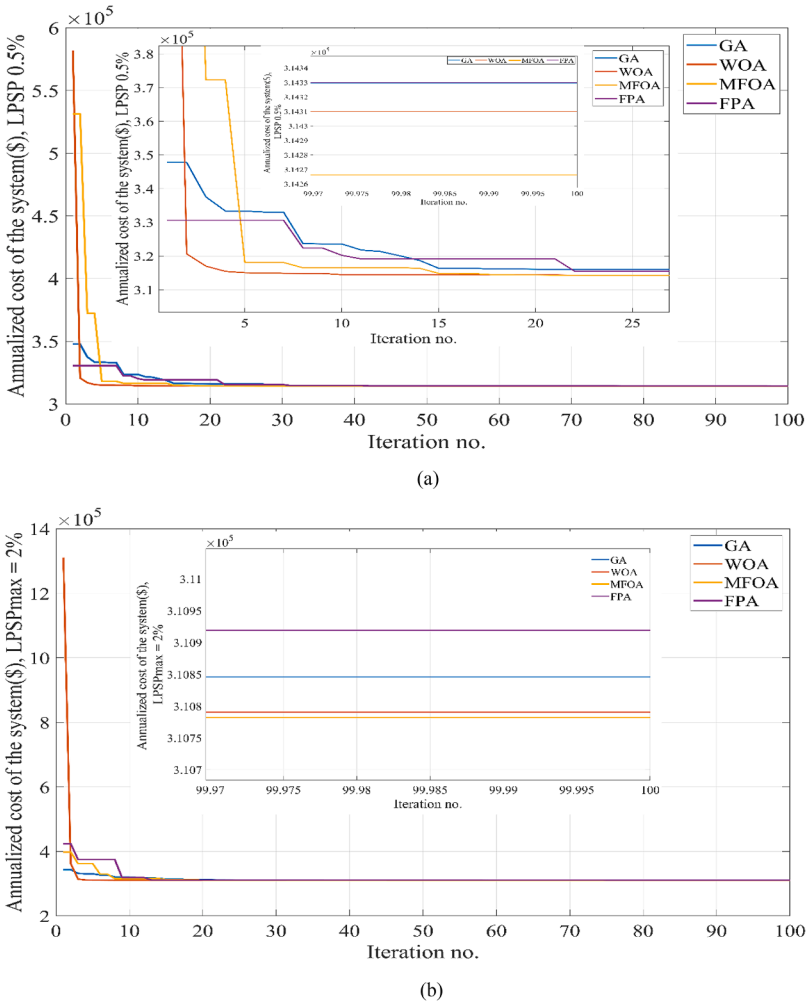

Fig. 23. Convergence analysis of ACS for LPSP (a) 0.5 %, (b) 2 %, (c) 5 %, (d) 10 %.

(b). The BT component was charged at a rate of 33.66 % in January; 36.92 % in February; 56.14 % in March; 83.66 % in April; over 90 % in May, June, July, and August; 87.62 % in September; 62.07 % in October; 26.5 % in November; and 21.67 % in December. In an HRES, the charge-discharge rates of the BT component should be continuously monitored. In this study, it was demonstrated that the SOC value of BT was generally good, with a few exceptions. Specifically, the months of January, November, and December showed deviations due to the scarcity of natural resources. The scarcity of natural resources during these months can be attributed to seasonal variations, where certain renewable resources such as solar or wind might be less abundant. Low solar radiation and wind speed values were observed in October, November, and December, leading to the SOC value of BT dropping by 20 % in these months, as depicted in the figures. A consistent and high SOC value for the BT ensures that the system operates efficiently, meeting the energy demands without straining the storage components. Fig. 16 shows that, in addition to the PV and BT components, the load demand in January, November, and December was primarily met by the energy purchased from the grid. Maintaining an optimal SOC value is vital not only for ensuring an uninterrupted energy supply but also for prolonging the life span and efficiency of the BT components in an HRES.

Fig. 20 provides information on the resources used to meet the hourly energy demand throughout the year (8760 h). More detailed and numerical data can be obtained by zooming into a graphical time series. Fig. 21 shows the time periods over the course of the year when the energy was drawn from and sold to the grid. In this figure, the annual energy value of 1.2114×10^6 kWh sold to the grid and 4.4086×10^5 kWh purchased from the grid are presented.

Figs. 22(a) and (b) present a weekly comparison analysis of the load, WT, PV, BT charge-discharge values, and energy purchased from the grid. The analyses focused on specific periods that were designated within the system's operation. As observed in the figures, the energy from the grid and the BT charge-discharge management processes worked in tandem to offset power fluctuations from renewable resources, ensuring that the load demand was consistently addressed. Generally, an elevation in the TNPC and COE values led to a significant reduction in the LPSP, highlighting the trade-off between system reliability and economic efficiency.

Tables 4, 5, and 6 present the optimal system sizing results derived using the MFOA, WOA, FPA, and GA optimization methodologies for distinct LPSP levels: 2 %, 5 %, and 10 %. A cursory examination reveals only marginal variations in parameters such as wind turbines, solar power, and BT units across the different optimization techniques. In contrast, parameters like total wind energy, total solar energy, and total load demand largely remain invariant. Importantly, all methodologies consistently yield an REF value of 100 %, emphasizing the uniform reliability of energy provision across these techniques.

A closer look at the economic indicators, particularly LCOE, grid sales, grid purchases, and TNPC, suggests that optimization techniques, when adjusted for a specific LPSP level, produce similar economic outcomes. This underscores the analogous economic performance rendered by these distinct methodologies and brings to light subtle variances in

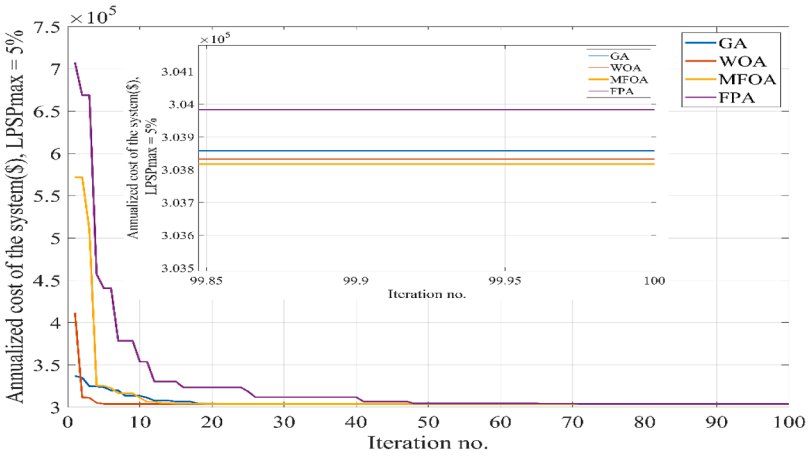

(c)

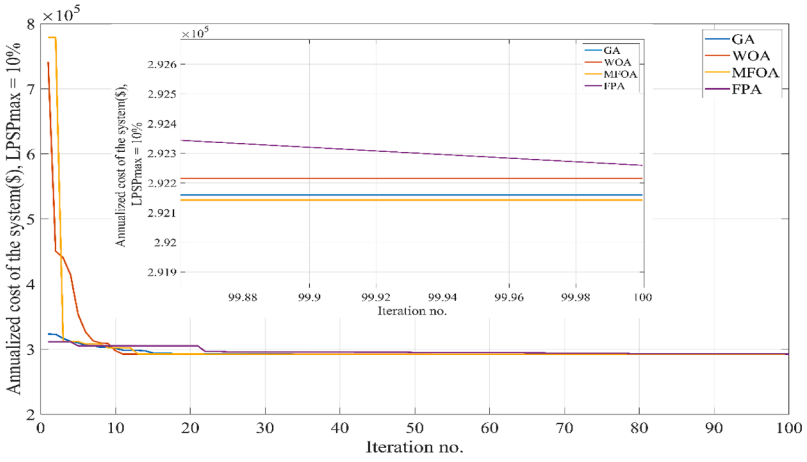

(d)

Fig. 23. (*continued*).

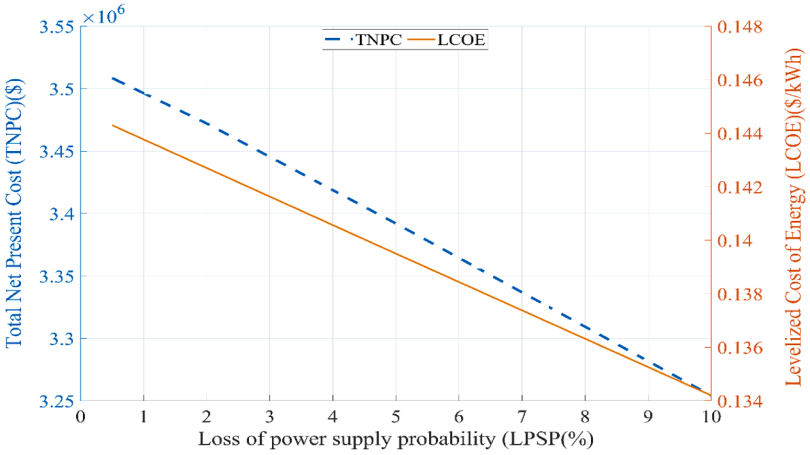

Fig. 24. Effect of different LPSP values on TNPC and LCOE.

sizing parameters influenced by different LPSP values.

In summary, the tables confirm that, based on a designated LPSP value, various optimization techniques produce comparable system-sizing outcomes. This congruence is most pronounced in the economic parameters, although slight differences in some sizing parameters are noticeable across LPSP values.

The results of the comparisons of the convergence performances of the algorithms at various LPSP values are shown in Fig. 23. In comparison to the other algorithms, WOA and MFOA exhibited a faster convergence towards the objective function, as seen in Figs. 23(a), (b), (c), and (d). WOA converged at the 10th iteration of the optimization process, whereas MFOA converged at the 13th iteration. After iteration number 26, MFOA surpassed WOA and quickly achieved the optimum outcome. Even though similar outcomes were attained, MFOA

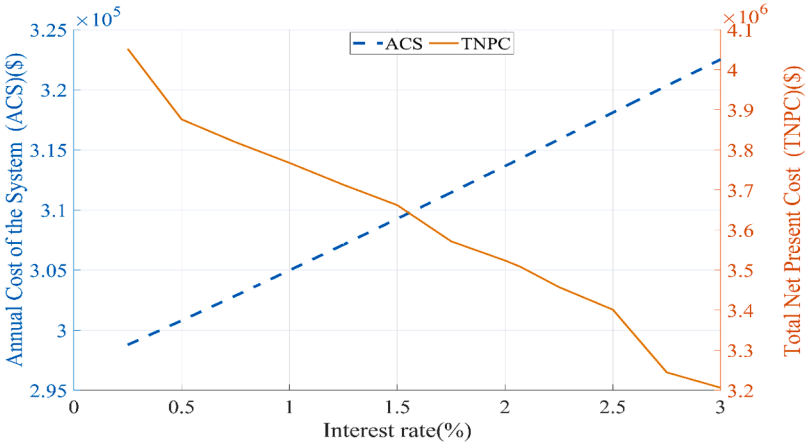

Fig. 25. Effect of different interests rate on ACS and TNPC.

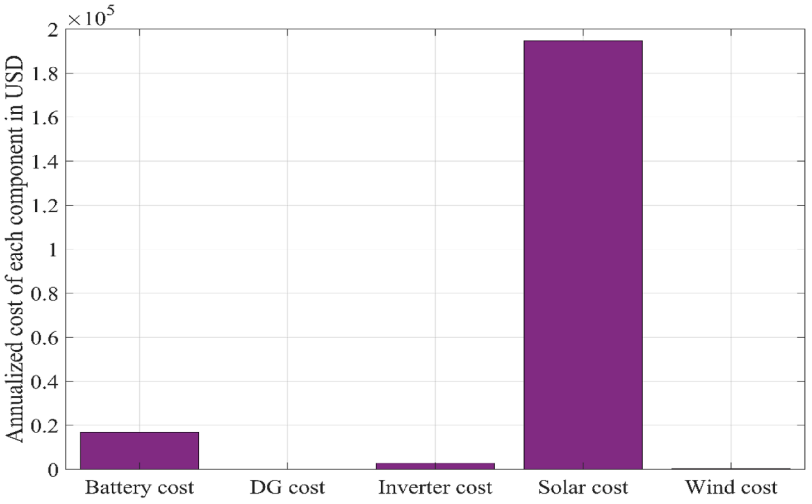

Fig. 26. Costs results of PV/WT/DG/BT for grid-connected HRES design.

completed the optimization process, as shown in Fig. 23(d), by achieving the lowest ACS, TNPC, and LCOE values and performing better than all other algorithms.

This convergence behavior confirms the superior exploitation capability of MFOA in the defined search space, reflecting its stability and robustness across varying reliability thresholds.

Fig. 24 illustrates the variations in TNPC and LCOE results for different LPSP values. An evident inverse relationship emerged between LPSP values and both LCOE and TNPC values. This inverse trend has important ramifications for understanding the interplay between system reliability (as indicated by the LPSP) and the economic feasibility of the energy system. Previous studies have often hinted at this relationship, but our findings provide a more nuanced understanding, especially in the context of our specific system setup. A sensitivity analysis focusing on interest rate changes was conducted to delve deeper into the economic intricacies of the system. The ensuing results, depicted in Fig. 25, show an increase in the ACS value, whereas the TNPC value exhibits a decline as the interest rate surges. This behavior underscores the delicate balance between financial parameters and system costs, a topic that has been a focal point in the RE finance literature. As interest rates reflect the time value of money and risk, their influence on RE system economics is pivotal, and our findings shed light on some of the subtle dynamics at play.

The comparison of economic and environmental outcomes across varying LPSP levels reveals a clear trade-off: as system reliability decreases (i.e., LPSP increases), economic performance improves through reduced LCOE and TNPC, while maintaining an REF of 100 %. This suggests that even when minor reliability compromises are introduced, the environmental sustainability of the system remains uncompromised. This indicates that economic savings can be achieved without compromising environmental integrity, provided that the system is properly constrained and configured. These observations underscore the system's robustness and suitability for practical implementation scenarios where budget constraints and sustainability targets must be balanced.

A cost comparison of the components of the optimized HRES was conducted, and the results are shown in Fig. 26. The proposed MFOA method produced the following optimal values: \$404.8825 for WT, \$1.7826 $\times 10^5$ for PV, \$1.2291 $\times 10^4$ for BT, \$3.0598 $\times 10^3$ for inverter, and \$2.9214 $\times 10^5$ for total annual cost.

6. Conclusions and future research directions

This study presented an advanced optimization approach based on the MFOA for the optimal design of a grid-connected HRES consisting of PV panels, WT, a DG, and BTS. The optimization framework incorporated the LPSP as a reliability constraint and aimed to minimize the TNPC by determining the optimal sizing of all system components. The results demonstrated that the MFOA consistently outperformed the other metaheuristic algorithms—namely, the WOA, FPA, and GA—in

terms of convergence speed, solution stability, renewable energy utilization, and computational efficiency across all evaluated LPSP levels. While the PV/WT/BT configuration at higher LPSP values (e.g., 10 %) yielded the absolute lowest LCOE of $0.1342/kWh, the MFOA achieved a fully renewable (REF = 100 %) solution without DG operation at an LCOE of $0.1443/kWh.

According to the results of this study, the LCOE of the grid-connected system was 33 % lower than that of the off-grid model. When LPSP was chosen as 0.5 %, the HRES showed values of TNPC: $3.5085 × 10^6, ACS: $3.1426 × 10^5, and $0.1443⁄kWh; when LPSP was chosen as 2 %, it showed values of TNPC: $3.4721 × 10^6, ACS: $3.1078 × 10^5, and $0.1427⁄kWh; when LPSP was chosen as 5 %, it showed values of TNPC: $3.3920 × 10^6, ACS: $3.0382 × 10^5, and $0.1395⁄kWh, and when LPSP was chosen as 10 %, it showed values of TNPC: $3.2542 × 10^6, ACS: $2.9214 × 10^5, and $0.1342⁄kWh. The analyses of different LPSP targets showed that as the LPSP values rose, the ACS, NPC, and LCOE values dropped. Additionally, profit was obtained by selling $1.2114 × 10^6 kWh of energy to the grid annually. In the optimal solutions obtained with MFOA, the DG was not used, and the load demand was fully satisfied with a 100 % renewable fraction, resulting in zero overall emissions.

Every algorithm employed in the study was able to assess trends toward the optimum results. When an algorithm approaches the optimum solution, the density of the search space can be controlled in a self-adaptive manner; alternatively, when it gets farther away from the optimum solution, it can be expanded to allow for the discovery of new search points. It is clear at this point that our proposed MFOA method produces results that are excellently competitive when it comes to resolving the HRES sizing problem. It is anticipated that it will also be applied to more difficult problems in future research.

In addition, this study highlights the effectiveness of the optimization methods explored, particularly for hybrid grid-connected renewable energy systems. While the findings provide a solid foundation for understanding system dynamics, further research is needed to explore the scalability and adaptability of these results across different environmental, economic, and technical settings. Future work could focus on integrating advanced stochastic models to account for uncertainties in renewable energy sources such as PV and wind, especially in regions with highly variable weather conditions. Moreover, examining the integration of emerging technologies like smart grids and the impacts of regulatory policies on renewable energy adoption would be valuable areas of exploration. The continued refinement of the MFOA algorithm to improve computational efficiency for larger, more complex systems, as well as its application to multi-objective optimization problems, could also be pursued. Finally, real-world implementation and validation of these optimization methods through pilot projects would provide insights into practical challenges and opportunities, helping policymakers and industry stakeholders better integrate renewable energy systems. These future directions present promising opportunities to further advance the design and efficiency of hybrid energy systems.

Funding

This work is derived from a research grant funded by the Research, Development, and Innovation Authority (RDIA), Kingdom of Saudi Arabia, with grant number 13382-psu-2023- PSNU-R-3-1-EI-. The authors would like to acknowledge the support of Prince Sultan University, Riyadh, Saudi Arabia in paying the article processing charges of this publication. This research is supported by the Automated Systems and Computing Lab (ASCL), Prince Sultan University, Riyadh, Saudi Arabia. In addition, the authors wish to acknowledge the editor and anonymous reviewers for their insightful comments, which have improved the quality of this publication.

Ethics declaration

Not applicable.

Ethics and consent to participate declarations

Not applicable.

Consent to publish declaration

Not applicable.

CRediT authorship contribution statement

Aykut Fatih Güven: Writing – original draft, Visualization, Validation, Supervision, Project administration, Methodology, Investigation, Formal analysis, Data curation, Conceptualization. **Onur Özdal Mengi:** Writing – review & editing, Visualization, Validation, Supervision, Project administration, Methodology, Investigation, Formal analysis, Conceptualization. **Mohit Bajaj:** Writing – review & editing, Visualization, Validation, Supervision, Software, Project administration, Methodology, Investigation, Formal analysis, Conceptualization. **Ahmad Taher Azar:** Writing – review & editing, Visualization, Validation, Supervision, Software, Project administration, Methodology, Funding acquisition, Formal analysis, Conceptualization. **Walid El-Shafai:** Validation, Supervision, Software, Methodology, Investigation, Funding acquisition, Formal analysis, Conceptualization.

Declaration of competing interest

The authors declare that they have no known competing financial interests or personal relationships that could have appeared to influence the work reported in this paper.

Acknowledgments

This work is derived from a research grant funded by the Research, Development, and Innovation Authority (RDIA), Kingdom of Saudi Arabia, with grant number 13382-psu-2023- PSNU-R-3-1-EI-. The authors would like to acknowledge the support of Prince Sultan University, Riyadh, Saudi Arabia in paying the article processing charges of this publication. This research is supported by the Automated Systems and Computing Lab (ASCL), Prince Sultan University, Riyadh, Saudi Arabia. In addition, the authors wish to acknowledge the editor and anonymous reviewers for their insightful comments, which have improved the quality of this publication.

Data availability

Data will be made available on request.

References

[1] M. Mehrpooya, M.M.M. Sharifzadeh, A novel integration of oxy-fuel cycle, high temperature solar cycle and LNG cold recovery - energy and exergy analysis, Appl. Therm. Eng. 114 (2017) 1090–1104, https://doi.org/10.1016/j.applthermaleng.2016.11.163.

[2] A.S. Bujang, C.J. Bern, T.J. Brumm, Summary of energy demand and renewable energy policies in Malaysia, Renew. Sustain. Energy Rev. 53 (2016) 1459–1467, https://doi.org/10.1016/j.rser.2015.09.047.

[3] A.M. Hemeida, A.S. Omer, A.M. Bahaa-Eldin, S. Alkhalaf, M. Ahmed, T. Senjyu, et al., Multi-objective multi-verse optimization of renewable energy sources-based micro-grid system: real case, Ain. Shams. Eng. J. 13 (2022) 101543, https://doi.org/10.1016/j.asej.2021.06.028.

[4] D. Temene Hermann, N. Donatien, T. Konchou Franck Armel, T. René, Techno-economic and environmental feasibility study with demand-side management of photovoltaic/wind/hydroelectricity/battery/diesel: a case study in Sub-Saharan Africa, Energy Convers. Manage 258 (2022), https://doi.org/10.1016/j.enconman.2022.115494.

[5] R. Sharma, H. Kodamana, M. Ramteke, Multi-objective dynamic optimization of hybrid renewable energy systems, Chem. Eng. Process - Process Intensif. 170 (2022) 108663, https://doi.org/10.1016/j.cep.2021.108663.

[6] A. Maleki, M.A. Rosen, Design of a cost-effective on-grid hybrid wind-hydrogen based CHP system using a modified heuristic approach, Int. J. Hydrogen. Energy 42 (2017) 15973–15989, https://doi.org/10.1016/j.ijhydene.2017.01.169.

[7] M.M. Samy, M.I. Mosaad, S. Barakat, Optimal economic study of hybrid PV-wind-fuel cell system integrated to unreliable electric utility using hybrid search optimization technique, Int. J. Hydrogen. Energy 46 (2021) 11217–11231, https://doi.org/10.1016/j.ijhydene.2020.07.258.
[8] A.F. Güven, N. Yörükeren, M.M. Samy, Design optimization of a stand-alone green energy system of university campus based on Jaya-Harmony Search and Ant Colony Optimization algorithms approaches, Energy 253 (2022), https://doi.org/10.1016/j.energy.2022.124089.
[9] A.F. Güven, M.M. Samy, Performance analysis of autonomous green energy system based on multi and hybrid metaheuristic optimization approaches, Energy Convers. Manage 269 (2022) 116058, https://doi.org/10.1016/j.enconman.2022.116058.
[10] A. Naderipour, H. Kamyab, J.J. Klemeš, R. Ebrahimi, S. Chelliapan, S.A. Nowdeh, et al., Optimal design of hybrid grid-connected photovoltaic/wind/battery sustainable energy system improving reliability, cost and emission, Energy 257 (2022), https://doi.org/10.1016/j.energy.2022.124679.
[11] G. Lei, H. Song, D. Rodriguez, Power generation cost minimization of the grid-connected hybrid renewable energy system through optimal sizing using the modified seagull optimization technique, Energy Reports 6 (2020) 3365–3376, https://doi.org/10.1016/j.egyr.2020.11.249.
[12] Y. Wang, J. Wang, L. Yang, B. Ma, G. Sun, N. Youssefi, Optimal designing of a hybrid renewable energy system connected to an unreliable grid based on enhanced African vulture optimizer, ISA Trans. 129 (2022) 424–435, https://doi.org/10.1016/j.isatra.2022.01.025.
[13] F.S. Mahmoud, A.A.Z. Diab, Z.M. Ali, A.H.M. El-Sayed, T. Alquthami, M. Ahmed, et al., Optimal sizing of smart hybrid renewable energy system using different optimization algorithms, Energy Reports 8 (2022) 4935–4956, https://doi.org/10.1016/j.egyr.2022.03.197.
[14] M.M.A. Seedahmed, M.A.M. Ramli, H.R.E.H. Bouchekara, A.H. Milyani, M. Rawa, F. Nur Budiman, et al., Optimal sizing of grid-connected photovoltaic system for a large commercial load in Saudi Arabia, Alexandria Eng. J. 61 (2022) 6523–6540, https://doi.org/10.1016/j.aej.2021.12.013.
[15] M.M. Samy, A. Emam, E. Tag-Eldin, S. Barakat, Exploring energy storage methods for grid-connected clean power plants in case of repetitive outages, J. Energy Storage 54 (2022) 105307, https://doi.org/10.1016/j.est.2022.105307.
[16] W. Chaichan, J. Waewsak, R. Nikhom, C. Kongruang, S. Chiwamongkhonkarn, Y. Gagnon, Optimization of stand-alone and grid-connected hybrid solar/wind/fuel cell power generation for green islands: application to Koh Samui, southern Thailand, Energy Reports 8 (2022) 480–493, https://doi.org/10.1016/j.egyr.2022.07.024.
[17] B. Sharma, M. Rizwan, P. Anand, A new intelligent approach for size optimization of a renewable energy based grid connected hybrid energy system, Int. J. Numer. Model. Electron. Networks, Devices Fields (2022) 1–19, https://doi.org/10.1002/jnm.3050.
[18] M.A. Ben Taher, B.E. Lebrouhi, S. Mohammad, E. Schall, T. Kousksou, Multi-objective optimization of a grid-connected PV system for a public building: faculty of Sciences and Technology at Pau, Clean. Technol. Environ. Policy. 24 (2022) 2837–2849, https://doi.org/10.1007/s10098-022-02364-4.
[19] M.C. Krstevska, P. Krstevski, M. Srbinovska, V. Andova, A.K. Mateska, Smart forecasting: enhancing virtual power plant performance with analytical frameworks. E-prime, Adv. Electr. Eng. Electron. Energy 12 (2025) 101003, https://doi.org/10.1016/j.prime.2025.101003.
[20] M.R.E. Rasekh, F.M. Sharifi, S. Alavi, N. Janatyan, Modeling solar power plant electricity supply chain toward renewable energy consumption, E-Prime - Adv. Electr. Eng. Electron. Energy 11 (2025) 100907, https://doi.org/10.1016/j.prime.2025.100907.
[21] B. Dey, G. Sharma, P.N. Bokoro, Incentive-based demand response policies for techno-economic microgrid operation—a Comparative analysis, Electr. Eng. (2025), https://doi.org/10.1007/s00202-025-03263-9.
[22] P. Tiam Kapen, Optimal multi-objective design of a photovoltaic/battery/wind hybrid system by implementing an innovative meta-heuristic algorithm, Clean. Energy Syst. 12 (2025) 100202, https://doi.org/10.1016/j.cles.2025.100202.
[23] M.A. Kamarposhti, H. Shokouhandeh, R. Outbib, I. Colak, E.M. Barhoumi, Techno-economic design of a hybrid photovoltaic-wind system for a residential microgrid considering uncertainties using dynamic parameters Bald Eagle algorithm, Int. J. Energy Res. 2025 (2025), https://doi.org/10.1155/er/5413946.
[24] D.F. Guedes Filho, R.L. Miranda, L.A. Correia, L. Do E. S.Fernandes, R.C. Medrado, M.D.C. Filho, et al., Optimization and integration strategies for hybrid renewable energy systems in the brazilian power grid: a systematic review, IEEe Access. 13 (2025) 84170–84187, https://doi.org/10.1109/ACCESS.2025.3569199.
[25] B. Mohammed, E.F. Amine, E.A. Nabil, Investigation of technoeconomic optimization for sizing renewable energy systems using metaheuristic and hybrid algorithms, Sci. African 28 (2025) e02712, https://doi.org/10.1016/j.sciaf.2025.e02712.
[26] S. Mohapatra, D. Kaliyaperumal, T. Porselvi, S.V.T. Sangeetha, R. Alroobaea, A. Emara, Optimal sizing of hybrid renewable energy systems relying on the black winged kite algorithm for performance evaluation, Sci. Rep. 15 (2025), https://doi.org/10.1038/s41598-025-06442-7.
[27] M. Jafari, A. Saeidavi, Optimizing fixed-tilt PV panel angles across diverse Iranian climates: a 200 kW techno-economic and environmental assessment, Next Res. 2 (2025) 100453, https://doi.org/10.1016/j.nexres.2025.100453.
[28] M.S. Hossain Lipu, M.S.A. Rahman, Z.U. Islam, T. Rahman, M.S. Rahman, S. T. Meraj, et al., Review of energy storage integration in off-grid and grid-connected hybrid renewable energy systems: structures, optimizations, challenges and opportunities, J. Energy Storage 122 (2025) 116629, https://doi.org/10.1016/j.est.2025.116629.
[29] L. Ouazzani Chahidi, Z. Bounoua, A. Mechaqrane, A novel hybrid machine learning approaches for prediction of greenhouse energy demand and production, E-Prime - Adv. Electr. Eng. Electron. Energy 11 (2025) 100944, https://doi.org/10.1016/j.prime.2025.100944.
[30] P.A. Gbadega, O.A. Balogun, Transactive energy management for efficient scheduling and storage utilization in a grid-connected renewable energy-based microgrid, E-Prime - Adv. Electr. Eng. Electron. Energy 11 (2025) 100914, https://doi.org/10.1016/j.prime.2025.100914.
[31] L. Jin, S. Zhong, B. Su, D. Zhou, Q. Wang, X. Yu, EV-integrated and grid-connected hybrid renewable energy system: a two-stage optimization strategy, Energy 330 (2025) 136858, https://doi.org/10.1016/j.energy.2025.136858.
[32] B. Suresh, K.E. Lakshmiprabha, U.A. Kumar, N.A. Natraj, Battery integration and grid-connected hybrid power plant with an optimal energy management system integrated into a multilevel configuration, J. Energy Storage 121 (2025) 116514, https://doi.org/10.1016/j.est.2025.116514.
[33] W. Zhu, J. Guo, G. Zhao, Multi-objective sizing optimization of hybrid renewable energy microgrid in a stand-alone marine context, Electron 10 (2021) 1–24, https://doi.org/10.3390/electronics10020174.
[34] A. Mahesh, K.S. Sandhu, Optimal sizing of a grid-connected PV/wind/battery system using particle swarm optimization, Iran. J. Sci. Technol. - Trans. Electr. Eng. 43 (2019) 107–121, https://doi.org/10.1007/s40998-018-0083-3.
[35] M.S. Javed, A. Song, T. Ma, Techno-economic assessment of a stand-alone hybrid solar-wind-battery system for a remote island using genetic algorithm, Energy 176 (2019) 704–717, https://doi.org/10.1016/j.energy.2019.03.131.
[36] L. Chen, S. Wang, N. Yousefi, An optimal arrangement for photovoltaic/diesel/battery management system applying Crow Search Algorithm: a case of Namib Desert, Int. J. Ambient. Energy 43 (2022) 4977–4989, https://doi.org/10.1080/01430750.2021.1909130.
[37] C. Ghenai, T. Salameh, A. Merabet, Technico-economic analysis of off grid solar PV/fuel cell energy system for residential community in desert region, Int. J. Hydrogen. Energy 45 (2020) 11460–11470, https://doi.org/10.1016/j.ijhydene.2018.05.110.
[38] R.G. Allwyn, A. Al-Hinai, R. Al-Abri, A. Malik, Optimization and techno-economic analysis of PV/battery system for street lighting using genetic algorithm - a case study in Oman, Clean. Eng. Technol. 8 (2022), https://doi.org/10.1016/j.clet.2022.100475.
[39] Y. Chen, R. Wang, M. Ming, S. Cheng, Y. Bao, W. Zhang, et al., Constraint multi-objective optimal design of hybrid renewable energy system considering load characteristics, Complex Intell. Syst. 8 (2022) 803–817, https://doi.org/10.1007/s40747-021-00363-4.
[40] M.F. Roslan, M.A. Hannan, P. Jern Ker, R.A. Begum, T.M. Indra Mahlia, Z.Y Dong, Scheduling controller for microgrids energy management system using optimization algorithm in achieving cost saving and emission reduction, Appl. Energy 292 (2021) 116883, https://doi.org/10.1016/j.apenergy.2021.116883.
[41] S. Ahmadi, S. Abdi, Application of the Hybrid Big Bang-Big Crunch algorithm for optimal sizing of a stand-alone hybrid PV/wind/battery system, Sol. Energy 134 (2016) 366–374, https://doi.org/10.1016/j.solener.2016.05.019.
[42] E.L.V. Eriksson, E.M.A. Gray, Optimization of renewable hybrid energy systems - a multi-objective approach, Renew. Energy 133 (2019) 971–999, https://doi.org/10.1016/j.renene.2018.10.053.
[43] F. Naseri, C. Barbu, T. Sarikurt, Optimal sizing of hybrid high-energy/high-power battery energy storage systems to improve battery cycle life and charging power in electric vehicle applications, J. Energy Storage 55 (2022) 105768, https://doi.org/10.1016/j.est.2022.105768.
[44] Y. Yang, S. Bremner, C. Menictas, M. Kay, Modelling and optimal energy management for battery energy storage systems in renewable energy systems: a review, Renew. Sustain. Energy Rev. 167 (2022) 112671, https://doi.org/10.1016/j.rser.2022.112671.
[45] H. Suryoatmojo, T. Hiyama, A.A. Elbaset, M. Ashari, Optimal design of wind-PV-diesel-battery system using genetic algorithm, IEEJ Trans. Power Energy 129 (2009) 413–420, https://doi.org/10.1541/ieejpes.129.413.
[46] B. Shi, W. Wu, L. Yan, Size optimization of stand-alone PV/wind/diesel hybrid power generation systems, J. Taiwan. Inst. Chem. Eng. 73 (2017) 93–101, https://doi.org/10.1016/j.jtice.2016.07.047.
[47] Yimen N., Tchotang T., Kanmogne A., Idriss I.A., Musa B., Aliyu A., et al. Optimal sizing and techno-economic analysis of hybrid renewable energy systems — a case study of 2020.
[48] V.J. Prakash, P.K. Dhal, Techno-economic assessment of a standalone hybrid system using various solar tracking systems for kalpeni island, india, Energies 14 (2021), https://doi.org/10.3390/en14248533.
[49] S.O. Sanni, J.Y. Oricha, T.O. Oyewole, F.I. Bawonda, Analysis of backup power supply for unreliable grid using hybrid solar PV/diesel/biogas system, Energy 227 (2021) 120506, https://doi.org/10.1016/j.energy.2021.120506.
[50] S. Barakat, H. Ibrahim, A.A. Elbaset, Multi-objective optimization of grid-connected PV-wind hybrid system considering reliability, cost, and environmental aspects, Sustain. Cities. Soc. 60 (2020), https://doi.org/10.1016/j.scs.2020.102178.
[51] A.K.S. Maisanam, A. Biswas, K.K. Sharma, Integrated socio-environmental and techno-economic factors for designing and sizing of a sustainable hybrid renewable energy system, Energy Convers. Manage 247 (2021) 114709, https://doi.org/10.1016/j.enconman.2021.114709.
[52] S. Jamshidi, K. Pourhossein, M. Asadi, Size estimation of wind/solar hybrid renewable energy systems without detailed wind and irradiation data: a feasibility study, Energy Convers. Manage 234 (2021) 113905, https://doi.org/10.1016/j.enconman.2021.113905.

[53] Case M.A., Kennel R., Abdelrahem M. Multiobjective optimization of a hybrid PV /wind / battery / diesel generator system integrated in 2022.
[54] H.O. Omotoso, A.M. Al-Shaalan, H.M.H. Farh, A.A Al-Shamma'a, Techno-economic evaluation of hybrid energy systems using artificial ecosystem-based optimization with demand side management, Electron 11 (2022), https://doi.org/10.3390/electronics11020204.
[55] J.L. Torres-Madroñero, C. Nieto-Londoño, J. Sierra-Pérez, Hybrid energy systems sizing for the colombian context: a genetic algorithm and particle swarm optimization approach, Energies 13 (2020) 1–30, https://doi.org/10.3390/en13215648.
[56] W.M. Hamanah, M.A. Abido, L.M. Alhems, Optimum sizing of hybrid PV, wind, battery and diesel system using lightning search algorithm, Arab. J. Sci. Eng. 45 (2020) 1871–1883, https://doi.org/10.1007/s13369-019-04292-w.
[57] V. Mukoro, M. Sharmina, A. Gallego-Schmid, A review of business models for access to affordable and clean energy in Africa: do they deliver social, economic, and environmental value? Energy Res. Soc. Sci. 88 (2022) 102530 https://doi.org/10.1016/j.erss.2022.102530.
[58] L. Suganthi, A.A. Samuel, Energy models for demand forecasting - a review, Renew. Sustain. Energy Rev. 16 (2012) 1223–1240, https://doi.org/10.1016/j.rser.2011.08.014.
[59] M. Chennaif, M. Maaouane, H. Zahboune, M. Elhafyani, S. Zouggar, Tri-objective techno-economic sizing optimization of off-grid and on-grid renewable energy systems using electric system Cascade Extended analysis and system Advisor Model, Appl. Energy 305 (2022), https://doi.org/10.1016/j.apenergy.2021.117844.
[60] D.E. Goldberg, K. Deb, in: G.J.E. RAWLINS (Ed.), A Comparative Analysis of Selection Schemes Used in Genetic Algorithms, A Comparative Analysis of Selection Schemes Used in Genetic Algorithms, 1, Elsevier, 1991, pp. 69–93, https://doi.org/10.1016/B978-0-08-050684-5.50008-2, editor.
[61] H.M. Pandey, A. Chaudhary, D. Mehrotra, A comparative review of approaches to prevent premature convergence in GA, Appl. Soft. Comput. J. 24 (2014) 1047–1077, https://doi.org/10.1016/j.asoc.2014.08.025.
[62] J.P. Ram, D.S. Pillai, A.M.Y.M. Ghias, N. Rajasekar, Performance enhancement of solar PV systems applying P&O assisted flower pollination algorithm (FPA), Sol. Energy 199 (2020) 214–229, https://doi.org/10.1016/j.solener.2020.02.019.
[63] X.-S. Yang, Nature-inspired Optimization Algorithms, Elsevier, 2014, https://doi.org/10.1016/C2013-0-01368-0.
[64] S. Mirjalili, A. Lewis, The whale optimization algorithm, Adv. Eng. Softw. 95 (2016) 51–67, https://doi.org/10.1016/j.advengsoft.2016.01.008.
[65] J.A. Goldbogen, A.S. Friedlaender, J. Calambokidis, M.F. McKenna, M. Simon, D. P. Nowacek, Integrative approaches to the study of baleen whale diving behavior, feeding performance, and foraging ecology, Bioscience 63 (2013) 90–100, https://doi.org/10.1525/bio.2013.63.2.5.
[66] H. Sun, A.G. Ebadi, M. Toughani, S.A. Nowdeh, A. Naderipour, A. Abdullah, Designing framework of hybrid photovoltaic-biowaste energy system with hydrogen storage considering economic and technical indices using whale optimization algorithm, Energy 238 (2022), https://doi.org/10.1016/j.energy.2021.121555.
[67] M. Shehab, L. Abualigah, H. Al Hamad, H. Alabool, M. Alshinwan, A. M Khasawneh, Moth-flame optimization algorithm: variants and applications, Neural Comput. Appl. 32 (2020) 9859–9884, https://doi.org/10.1007/s00521-019-04570-6.

AYKUT FATİH GÜVEN was born in Tarsus, Turkey, in 1979. He received the B.S. and M.S. degrees in electrical engineering from Karadeniz Technical University, Trabzon, Turkey, in 2000 and 2004, respectively, and the Ph.D. degree in electrical engineering from Kocaeli University, Kocaeli, Turkey, in 2022. Since 2023, he has been serving as an Assistant Professor in the Department of Electrical and Electronics Engineering at Yalova University, Yalova, Turkey. His research focuses on renewable energy, hybrid energy systems management, electrical vehicles, control systems, power system analysis, artificial intelligence, and meta-heuristic optimization.

Onur Ozdal Mengi received a BS degree in electrical and electronics engineering from Firat University, Elazig, Turkey, in 2000 and a MS degree and a PhD degree in electrical and electronics engineering from Karadeniz Technical University, Trabzon, Turkey, in 2004 and 2011, respectively. He worked at Giresun University, Giresun, Turkey, from 2002 to 2019. He has been working as professor in the Department of electrical and electronics engineering at Giresun University since 2024. He has published many papers in journals, and national and international conferences. His current research interests include control systems, renewable energy, energy management, and power electronics.

Mohit Bajaj is a Research Professor in the Department of Electrical Engineering at Graphic Era (Deemed to be University) in Dehradun, India. With a Ph.D. in Electrical Engineering from the prestigious National Institute of Technology in Delhi, he has established himself as a distinguished scholar and researcher in his field. Fueled by a passion for innovation and sustainability, Dr. Bajaj's primary research interests revolve around electric vehicles, renewable energy sources, distributed generation, power quality, and smart grids. His extensive contributions to the field are evidenced by his numerous research publications, comprising impactful journal articles, international conference papers, and book chapters. With a commitment to international collaboration, Dr. Bajaj actively engages with researchers in the renewable energy domain, fostering partnerships with esteemed institutions and scholars from various countries. Furthermore, Dr. Bajaj's exceptional contributions have garnered global recognition. He is ranked among the World's Top 2 % Scientists for the three consecutive years according to a recent study conducted by researchers from ICSR Lab, Elsevier B.V., and Stanford University in 2021, 2022 and 2023, reaffirming his status as a prominent figure in the field of Electrical Engineering. Through his relentless pursuit of knowledge, extensive research contributions, and commitment to academic collaboration, Dr. Mohit Bajaj continues to shape the future of renewable energy and electrical engineering, leaving an indelible impact on the scientific community and inspiring the next generation of researchers.

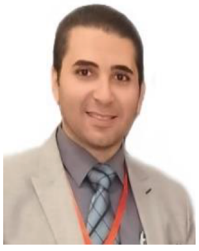

Ahmad Taher Azar (Senior Member, IEEE) is a full Professor at College of Computer and Information Sciences (CCIS), Prince Sultan University, Riyadh, Saudi Arabia. He is a leader of Automated Systems and Computing Lab (ASCL), Prince Sultan University, Saudi Arabia. He is currently an editor for IEEE Systems Journal, IEEE Transactions on Neural Networks and Learning Systems, Springer's Human-centric Computing and Information Sciences, and Elsevier's Engineering Applications of Artificial Intelligence. Prof. Azar has expertise in Artificial Intelligence, Control Theory and Applications, Robotics, Machine Learning, Computational Intelligence and dynamical system modeling. He has authored/co-authored over 500 research papers in prestigious peer-reviewed journals, book chapters, and conference proceedings.

Walid El-Shafai (Senior Member, IEEE) was born in Alexandria, Egypt. He received his B.Sc. degree with honors in Electronics and Electrical Communication Engineering from the Faculty of Electronic Engineering (FEE), Menoufia University, Menouf, Egypt, in 2008. He earned his M.Sc. degree from the Egypt-Japan University of Science and Technology (E-JUST) in 2012 and his Ph.D. degree from the FEE, Menoufia University, in 2019. From January 2021 to December 2024, He was a researcher with the Security Engineering Laboratory (SEL) at Prince Sultan University (PSU), Riyadh, Saudi Arabia. He currently serves as a Senior Researcher at the Automated Systems and Computing Lab (ASCL) and as an Assistant Professor at the College of Computer Science and Information Systems, PSU, Riyadh. In addition, he is an Associate Professor with the Department of Electronics and Communication Engineering (ECE) at the Faculty of Electronic Engineering, Menoufia University. His research interests encompass a broad range of fields, including wireless mobile and multimedia communication systems, image and video signal processing, efficient 2D/3D video coding and transmission, quality of service and experience, digital communication techniques, cognitive radio networks, adaptive filter design, 3D video watermarking, steganography, encryption, error resilience and concealment algorithms for video codecs (H.264/AVC, H.264/MVC, and H.265/HEVC), cognitive cryptography, medical image processing, speech processing, security algorithms, software-defined networks, the Internet of Things, FPGA implementations of signal processing algorithms and communication systems, cancellable biometrics, pattern recognition, image and video magnification, artificial intelligence applications in signal processing and communication systems, modulation identification and classification, image and video super-resolution and denoising, automated systems, cybersecurity applications, malware and ransomware detection, and deep learning for signal processing and communication systems. He is a dedicated reviewer for numerous international journals and conferences, contributing to the advancement of research in his areas of expertise.